Construction and Building Materials 418 (2024) 135307

Contents lists available at ScienceDirect

Construction and Building Materials

journal homepage: www.elsevier.com/locate/conbuildmat

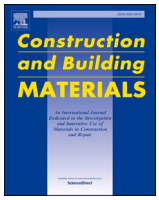

Uni- and tri-axial tests and property characterization for thermomechanical effect on hydrated lime modified asphalt concrete

Azedin Al Ashaibi [a], Yu Wang [a,*], Amjad Albayati [b], Laurence Weekes [a], Jonathan Haynes [a]

[a] School of Science, Engineering & Environment, University of Salford, Manchester, UK
[b] Department of Civil Engineering, University of Baghdad, Iraq

ARTICLE INFO

Keywords:
Hydrated lime mineral filler
Hot mix asphalt concrete
Pavement permanent deformation
Resilient modulus

ABSTRACT

Permanent deformation, fatigue and thermal cracking are the three typical distresses of flexible pavement. Using hydrated lime (HL) into the conventional limestone mineral additive has been widely practiced, including in Europe, to improve the mechanical properties of hot mix asphalt (HMA) concrete and as the result the durability of the constructed pavement. Large number of experimental studies have been reported to find the optimum addition of HL for the improvement on HMA concrete mechanical properties, moisture susceptibility and fatigue resistance. Pavement in service is under complex thermomechanical stress-strain conditions due to coupled atmospheric and surrounding environment temperature variation and the traffic loading. To predict and analyse the performance of pavement structures the data only from uniaxial compressive test for the resilient modulus and permanent deformation would be not enough. However, so far, the data of HL modified HMA concrete under complex loading conditions are still not well informatively complete. To contribute new knowledge, this paper reports an experimental study of both uni- and tri-axial tests for the asphalt concrete using HL into mineral additive for the mixes designed for the applications of wearing, levelling, and base layers, respectively. All the tests were conducted under three controlled temperatures and four stress deviations. The test results have showed that, for all three types of mixes, the permanent deformation of the HL mixes is less than the ones of no HL addition. The degree of the improvement on permanent deformation resistance using HL is much pronounced at high stress deviation states. The results have also showed that the resilient modulus strongly depends on the temperature and stress deviation while the mixes of HL addition demonstrate higher rigidity. At last, mathematical characterization models have been proposed for the measured material properties. A numerical simulation case study has been performed to test and demonstrate the application of the proposed unified property model.

1. Introduction

Rutting or permanent deformation is one of the most common distresses for asphalt pavements [1]. It is due to inadequate shear strength within pavement when exposed to high temperatures and repetitive traffic load [2,3]. Asphalt concrete mixture design and its composite material modification play the primary effective role to improve asphalt pavement rutting resistance [4]. For example, layer structure design and construction influence the high-temperature performance of asphalt pavement because their effects on the heat dissipation and retention of the whole structure [5]. On the other hand, modifying asphalt concrete using mineral additives to be the micro-filler has been widely adopted and proven effective to improve flexible pavement durability [6]. Among the varied functional mineral additives, hydrated lime (HL) has been of particular interest due to its chemical activity comparing with other mineral additives, such as fly ash, limestone dust, and lower energy consumption than cement. Previous studies have proven that partial replacement of the conventional limestone filler using HL at the rate of 2.5% by the total aggregate weight produced optimistic improvement on the resistance of Hot Mix Aspahlt (HMA) concrete to permanent deformation [7], moisture susceptibility [8] and fatigue distress [9].

Rutting resistance of asphalt concrete is determined by both the bitumen binder rheology and the angle of friction between aggregate particles. Two parameters called the rutting parameter, G* /sinδ, and zero-shear viscosity (ZSV) are commonly used for the binder rheological effect [10,11]. For final asphalt concrete mixtures, the flow number

* Corresponding author.
E-mail address: y.wang@salford.ac.uk (Y. Wang).

https://doi.org/10.1016/j.conbuildmat.2024.135307
Received 13 July 2023; Received in revised form 10 December 2023; Accepted 31 January 2024
Available online 14 February 2024

Table 1
the key Marshall properties of the asphalt concrete mixes.

Mixes	Limestone dust (%)	HL (%)	OAC (%)	Density (g/cm3)	AV (%)
CW	7	0	4.9	2.34	4.02
CL	6	0	4.6	2.32	4.02
CB	5	0	4.3	2.31	4.29
HL 2.5 W	4.5	2.5	5.3	2.32	4
HL 2.5 L	3.5	2.5	5	2.3	4.5
HL2.5B	2.5	2.5	4.6	2.3	4.39

parameter has been proposed to assess their rutting potential [12,13]. Both uniaxial and triaxial penetration tests are commonly used to evaluate the flow number for the performant deformation behaviour of asphalt concrete [14], for which, triaxial repeated load permanent deformation test can not only check the quality of mixture design, but also provide realistically conditional parameters for design and analysis to predict the rutting depth of asphalt pavement [15–17] and the variation of the resilient modulus [18] under complex service conditions, as well as the thermomechanical behaviours of asphalt concrete [19].

In spite of large number of laboratory and field studies on the HL modified asphalt concrete [20,21], specific investigation on its rutting behaviour is still insufficient. Particularly, the knowledge of the material plastic and elastic properties under complex coupled climatic thermal and traffic mechanical conditions is still limited. There is, so far, little experimental research on triaxial tests for HL modified asphalt concrete. Most of the reported work on the characterization for the properties in response to the coupled thermomechanical influence is not enough to provide fully supportive guidance for pavement design trying to use the HL modified asphalt concrete [22,23]. To contribute more knowledge to fill the gap, this paper reports an experimental study on both uni- and tri-axial tests to compare the elastoplastic behaviour, under coupled thermal and mechanical loads, of HMA concrete mixtures with and without HL modification. The measurements of permanent deformation and resilient modulus have been characterized for their variation with the complex stress states, temperature and the types of mix.

2. Experiment

Asphalt concrete mixes were made following the design standard [24] for three pavement layers, i.e., Wearing, Leveling and Base courses. At first, three control mixes which use limestone dust ($CaCO_3$) only for the mineral filler (MF) were made. The particle size of the limestone dust is less than 0.075 mm (passed through sieve No. 200). The MF contents are 7%, 6%, and 5% by total weight of the mix for the Wearing, Leveling and Base mixes, respectively. Thereafter, three other counterpart modified mixes were made to use hydrated lime ($Ca(OH)_2$) to replace the limestone dust by 2.5% of the total weight of the aggregates of each control mix. Table 1 gives out the three key Marshall property values of the designed total six mixes, they are the optimum asphalt cement (OAC) content, bulk density, and air void (AV) content [7]. It shows that HL modified mixes have a higher OAC and AV in general. More information about the aggregate and filler materials has been provided in the appendix.

Fig. 1 displays the experimental setup for both uni- and tri-axial tests. The prepared six mixes were casted into cylindrical specimens by triplicate. All tests were conducted by triplicate. The present data are the average of the three repetitive tests. The specimens have a size of 101.6 mm (4 in.) in diameter and 152.4 mm (6 in.) in height. Specimens were put into an airtight pressure cell, in which a peripheral confining pressure on the cylindrical side surface was applied, meanwhile a vertical axial compressive load exists on the top of the sample. The surface of the specimens was airproofed. The pressure cell and the specimen together were put into an environment chamber of a controlled temperature, and left there for at least two hours to reach a thermal equilibrium state.

The uni- and tri-axial tests were performed by applying a repetitive axial compressive loading (load stress) in the form of a rectangular wave with a frequency of 1 Hz, i.e., a certain load for 0.1 s followed by a rest without load for 0.9 s. All the tests were conducted under 3 controlled temperatures, they are 20, 40 and 60 °C. Each test had the total load repetition number up to 10,000. The deformation in the axial direction of the specimen was recorded using two LVDTs. The confining pressure (confining stress) was applied by the controlled static air pressure in the pressure cell. Using air pressure instead of traditional hydraulic pressure to provide confining pressure for triaxial tests had been employed to study the effects of loading speed, raw material types, and asphalt content on the shear strength of asphalt mixtures [25,26]. Total four loading conditions were conducted in this work, which are listed in the Table 2. One of the uniaxial tests was conducted in another study in the

Table 2
The triaxial test load conditions.

Deviatoric Stress psi (kPa)	Confining Stress, σ_3, psi (kPa)	Axial load Stress, σ_1, psi (kPa)
10 (68.9)	0 (0)	10 (68.9)
20 (137.9)*	0 (0)	20 (137.9)
20 (137.9)	10 (68.9)	30 (206.8)
30 (206.9)	10 (68.9)	40 (275.8)

* work conducted by Al-Tameemi et al. [7].

(a) Airtight pressure cell (b) Triaxial test under controlled temperature

Fig. 1. Triaxial experiment setup.

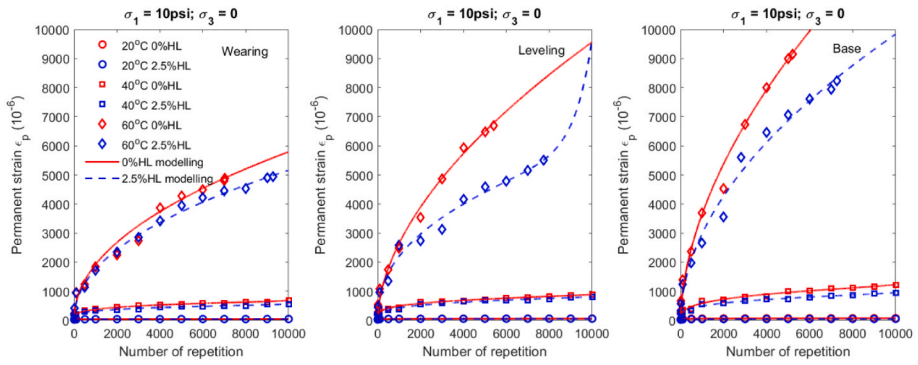

(a) Axial stress (σ_1) is 10 psi (68.9 kPa), confining stress (σ_3) is 0

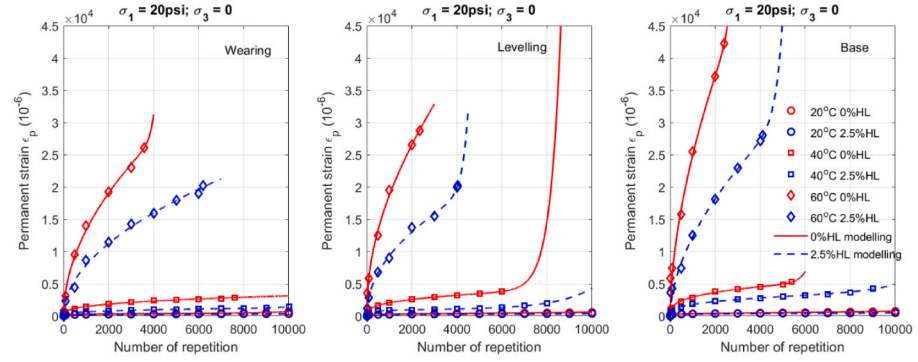

(b) Axial stress (σ_1) is 20 psi (137.9 kPa), confining stress (σ_3) is 0

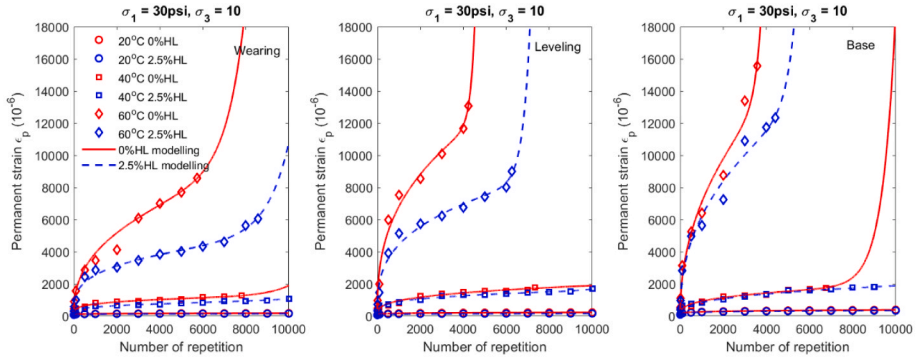

(c) Axial stress (σ_1) is 30 psi (206.9 kPa), confining stress (σ_3) is 10 psi (68.9 kPa)

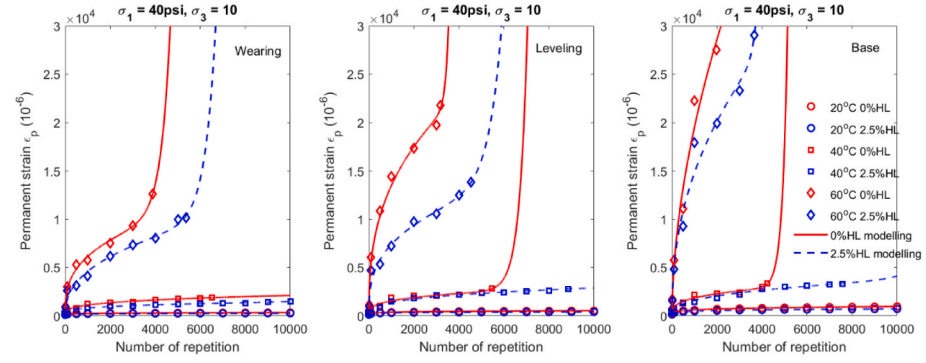

(d) Axial stress (σ_1) is 40 psi (275.8 kPa), confining stress (σ_3) is 10 psi (68.9 kPa)

Fig. 2. Permanent strain vs number of load repetition and the Franken ε_p-N representative curve.

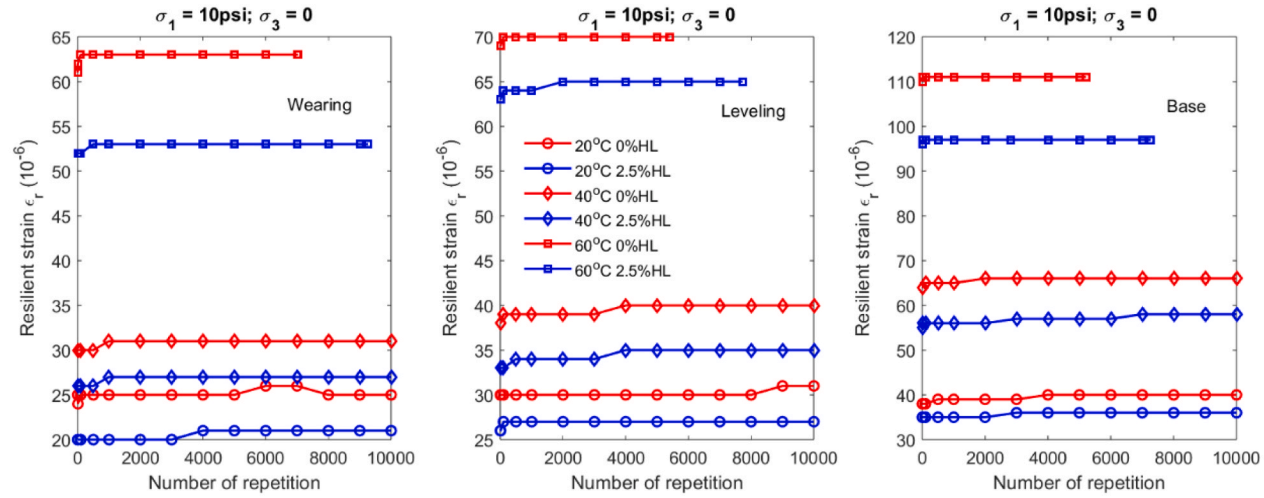

(a) Axial stress (σ_1) is 10 psi (68.9 kPa), confining stress (σ_3) is 0

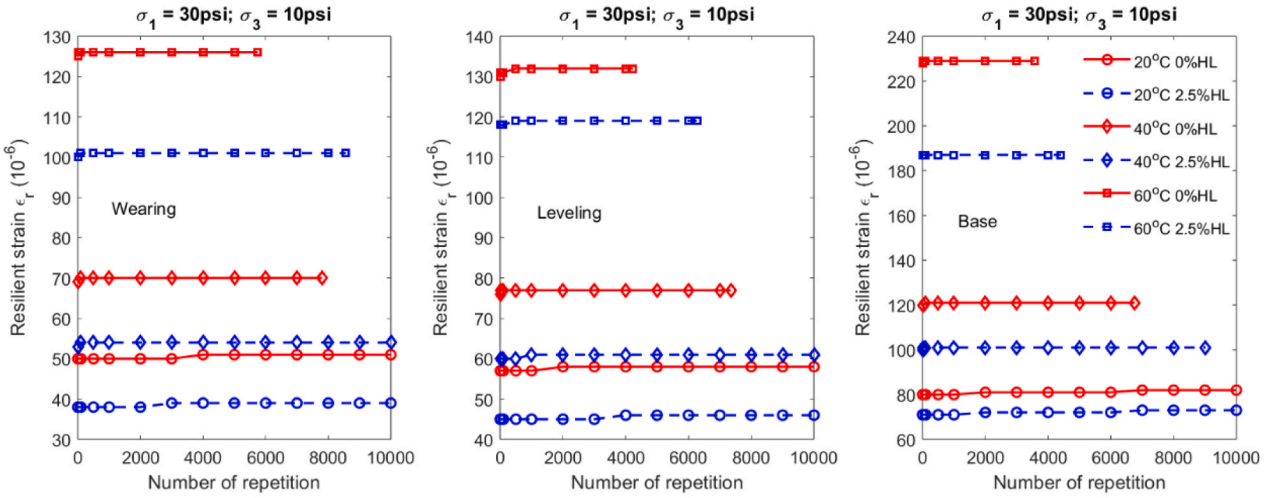

(b) Axial stress (σ_1) is 30 psi (206.9 kPa), confining stress (σ_3) is 10 psi (68.9 kPa)

Fig. 3. Axial elastic strain.

same serial research.

3. Experiment results and characterization

Both the permanent and elastic deformation have been recorded for the number of load repetition at 1, 2, 10, 100, 500, 1000, 2000, 3000, 4000, 5000, 6000, 7000, 8000, 9000 and 10,000. Fig. 2 shows the measured axial permanent strain (ε_p) under the four load conditions. Temperature presents distinctive influence on permanent deformation. The higher the temperature the larger the permanent deformation. The results in Fig. 2 demonstrate that, in general under the four loading conditions, increasing mineral filler (MF) content improves the rutting resistance since the permanent deformation of the three types of mix displaces a trend: that of wearing layer mix (7% MF) < that of levelling layer mix (6% MF) < that of base layer mix (5% MF). For all the mixes under the four loading conditions, the HL modification displaces more distinctive effect on stability improvement when exposed to high temperature.

The curve of permanent strain vs the number of the load repetition (ε_p-N) in general presents three distinctive stages [27], they are: 1). an initial stage of consolidation; 2). a secondary stage of a slow and stable rate of deformation accumulation, where the curve presents a nearly linear trend; and 3). a tertiary stage dominated by shear deformation. The number of cyclic load repetition, which corresponds the start of the tertiary stage, is called the flow number (Fn), when the slope of the curve begins to sharply increase. The Francken model, Eq. (1), has commonly adopted to represent the experimental ε_p-N curve measured in laboratory as it can catch up the three stage characteristics and identify the Fn [14]. The modelling curves in Fig. 2 shows that the Francken model well represents all the measured ε_p-N relationship. The modelling curves distinct the Fn, which shows that the HL modification largely increases the Fn when compared with that of the counterpart control mixes, particularly at high temperature.

$$\varepsilon_p = aN^b + c(e^{dN} - 1) \tag{1}$$

where ε_p is the performant strain, N stands the number of repetitions, a, b, c and d are four constant parameters.

Fig. 3 illustrates two examples of the measured axial resilient strain (ε_r) under a uniaxial and a triaxial loading conditions, respectively. Rather than hardening, the resilient strain shows increasement after exposed to initial numbers of load repetition. Such initial decrease of stiffness/rigidity can be explained due to initial shakedown of the mixes.

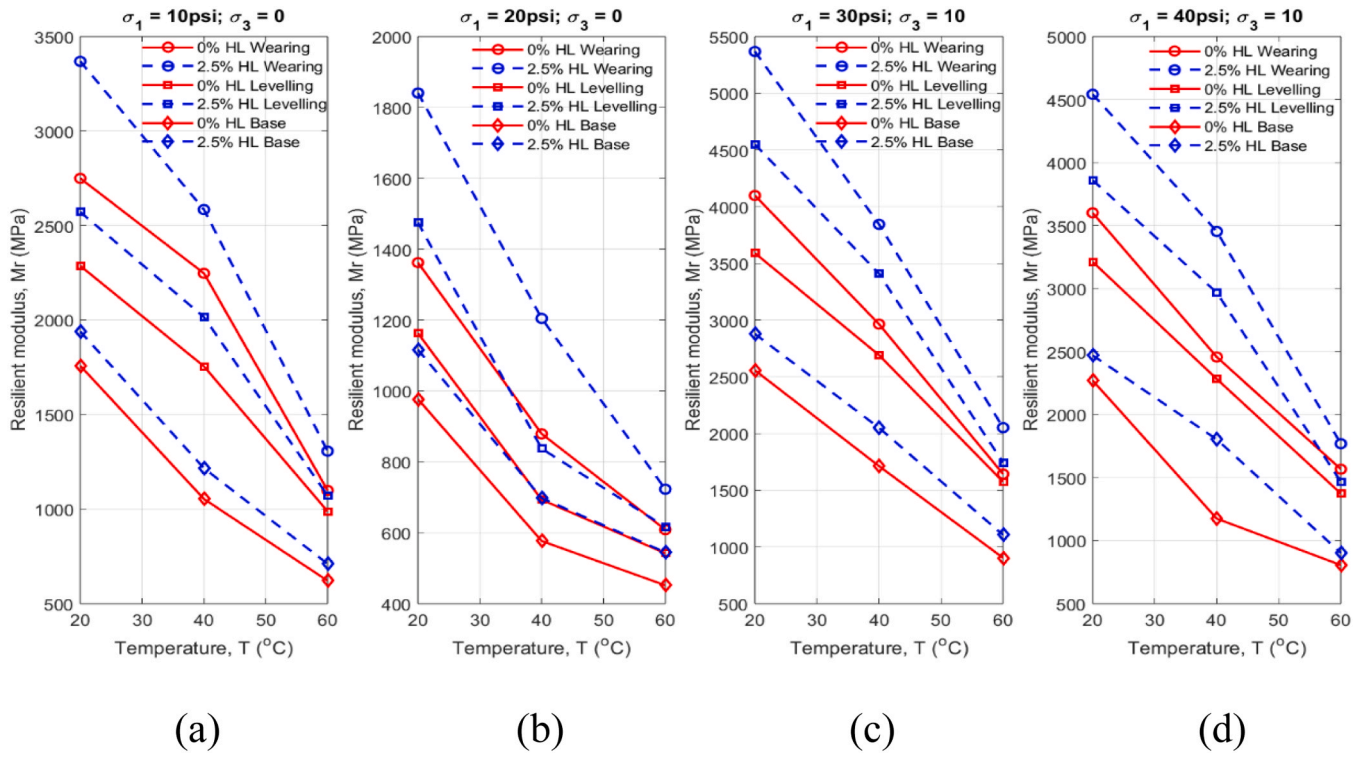

Fig. 4. Resilient modulus vs Temperature.

When subjected to cyclic or repeated loads elastoplastic structures could respond in a resilient manner when the load applied is above the yield limit but lower than a critical load limit [28,29]. Aligning with accumulated plastic deformation there exists local aggregate rearrangement within flowing asphalt matrix, which improves even mix of aggregate with asphalt paste. It can be noticed that the shakedown effect diminishes when confining stress is applied. Fig. 3 also shows that the increase of resilient strain due to the shakedown effect is too small to have a significant effect on the average value when calculating the average resilient modulus for each curve.

Fig. 4 shows the calculated average axial resilient modulus, $M_r = \frac{\sigma_1}{\bar{\varepsilon}_r}$, $\bar{\varepsilon}_r$ is the average of the axial resilient strain measurement in the Fig. 3. The data of Fig. 4(b) is from another early part of this series of research conducted at the same laboratory following the same procedure [7]. The results in Fig. 4 show that for all the mixes the resilient modulus considerably influenced by temperature. The higher the temperature the lower the modulus. The HL modification improves the stiffness/rigidity of the asphalt concrete, enhancing the resilient modulus value at all three temperatures.

Fig. 5 compares the resilient modulus under the four loading states when exposed to the same temperature. It can be noticed that resilient modulus is not a constant but depends upon the axial stress (σ_1) and the confining stress (σ_3). Under the same confining state, the higher the axial stress (σ_1) the lower the resilient modulus. Conversely, the confining stress increases the resilient modulus.

4. A unified characterization model for the deformation properties

For the sake of pavement design and structural analysis, a full integrated thermomechanical characteristic model is a necessary tool required for numerical modelling and simulation to predict permanent deformation. For this purpose, the obtained parametric values of the Francken modelling shown in Fig. 2 for permanent deformation, and the resilient modulus measurements in Figs. 4 or 5 need further investigation to characterise the effects of temperature and the stress states on the two mechanical properties. Naturally, the temperature and stress state are two independent variables for their coupled effect on the material properties. In addition, under complex conditions, the stress state itself has its own independent directional components. Seeing that the permanent deformation or rutting and the resilient modulus has a certain direction of interest in calculation, commonly in vertical direction of pavement structures, the two mechanical properties, residual modulus and permanent deformation, depend upon a local shear stress state, which is unable to be defined using a single parameter, such as either the stress invariants (I_1, I_2 or I_3) or deviatoric stress invariants (J_1, J_2 or J_3), but have to consider both the loading and confining conditions [30].

4.1. Resilient modulus, M_r

A mathematical expression for granular material resilient modulus under the triaxial stress conditions has been suggested [31], which can be simplified as:

$$M_r = k \quad {\sigma_1}^m {\sigma_3}^n \tag{2}$$

where, M_r is the resilient modulus, k is a material parameter relevant to the atmospheric pressure and void ratio, m and n are two material parameters. σ_1 is the axial stress, σ_3 is the confining pressure. The Eq. (2) has also been adopted for asphalt concrete [32]. A more general form of the Eq. (2) has also been suggested using the 1st and 2nd stress invariants to define the stress conditions, replacing the σ_1.and σ_3, respectively [33]. However, Eq. (2) has a limitation as it is unable to represent a uniaxial condition when confining pressure is zero. In addition, for the revised form, using the 1st and 2nd stress invariants to represent stress condition will overestimate the tensile stress effect as asphalt is weak in tensile comparing under compression. At last, our research also has found that the Eq. (2) brings in high nonlinearity that presented a challenge for the numerical solver. For the reasons, this research proposed a new characteristic model for the resilient modulus of asphalt concrete, which inclusively represents both the uni- and triaxial stress states as in the form of the Eq. (3),

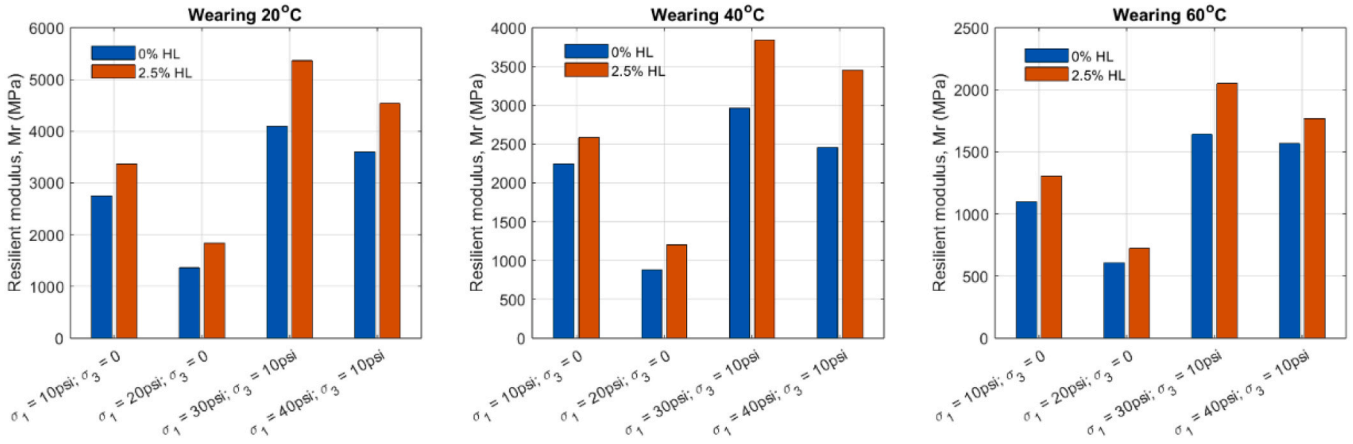

(a) Wearing mixes

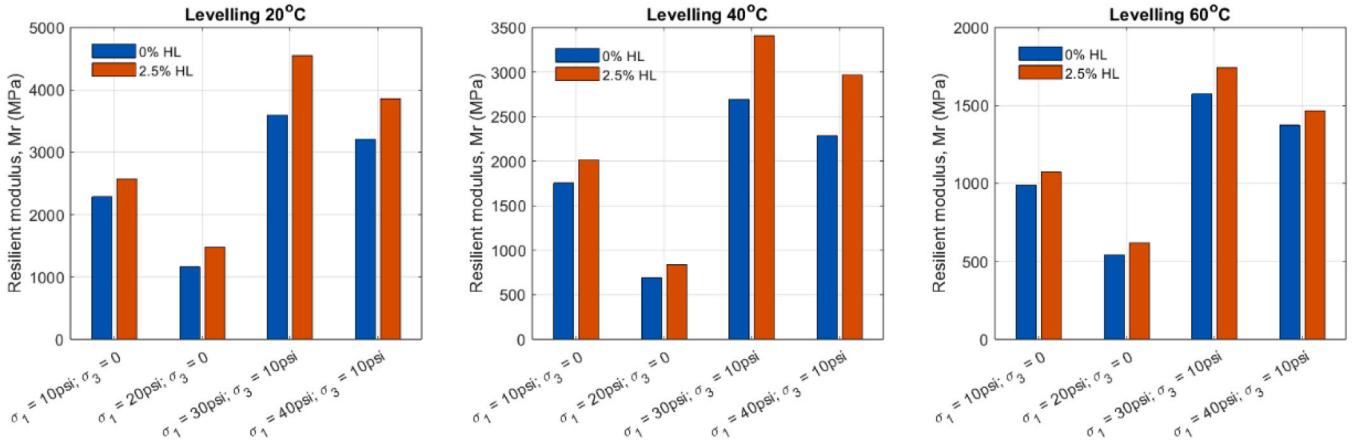

(b) Levelling mixes

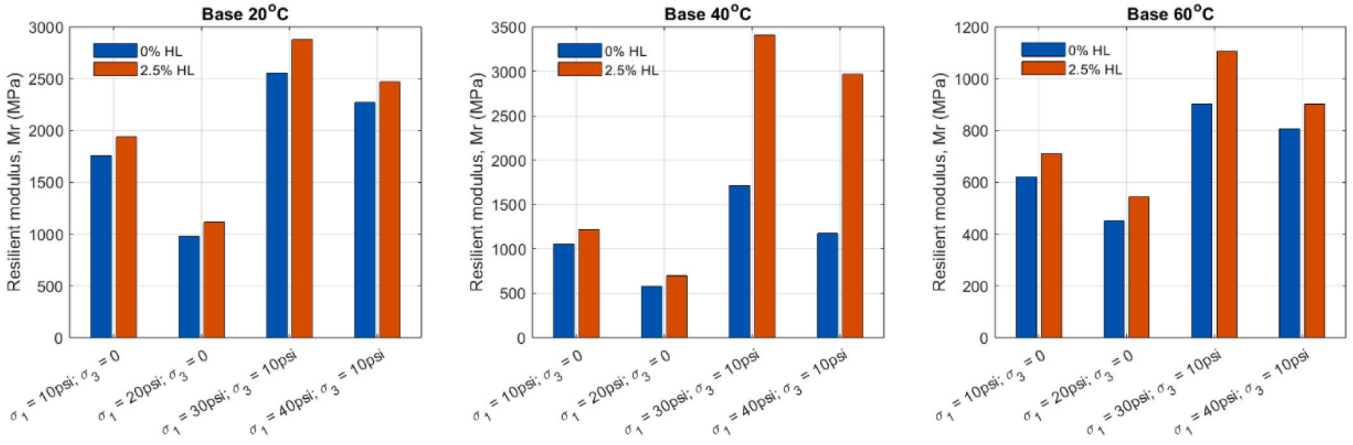

(c) Base mixes

Fig. 5. Comparison of the resilient modulus under different loading states.

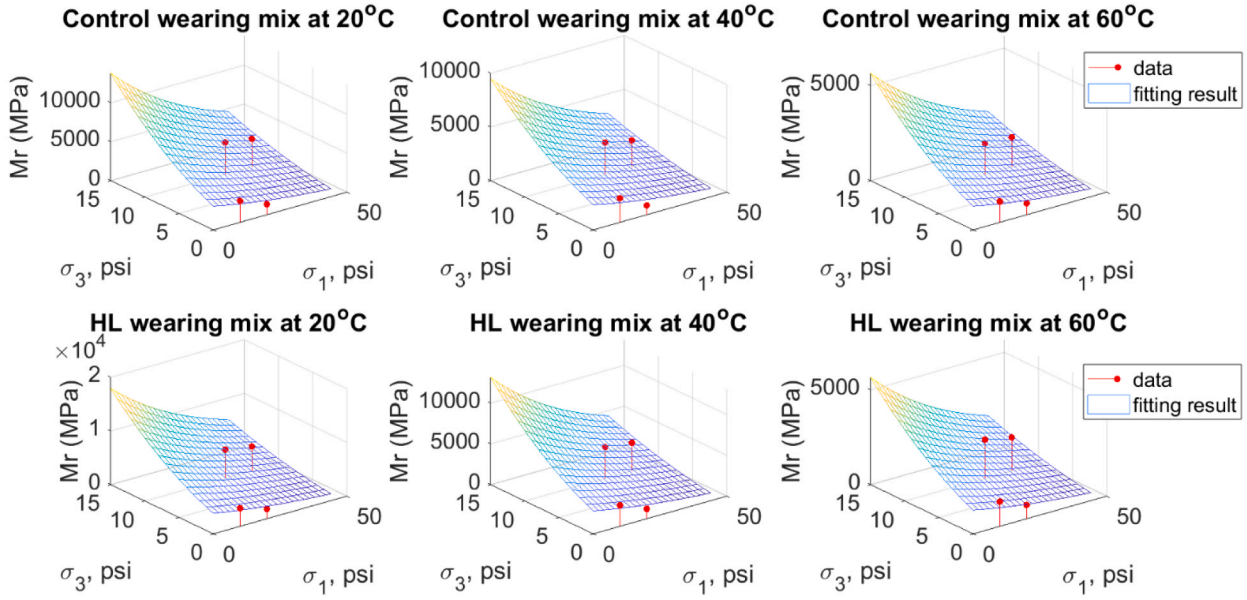

(a) The represented Mr characteristic surface

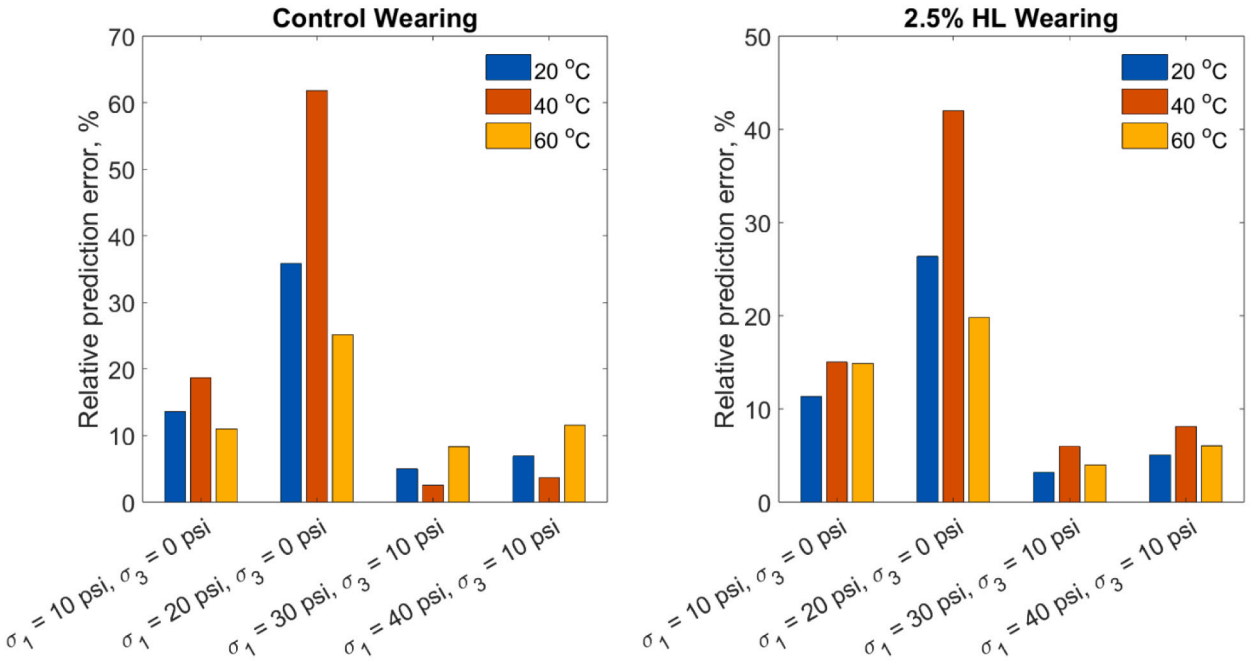

(b) The modelling relative error at the measurement points

Fig. 6. Modelling results of Eq. (3) for the Wearing mixes.

$$M_r = e^{a\sigma_1}(b+\sigma_3)^n \quad (3)$$

where σ_1 stands for primary (axial) compressive stress, σ_3 the secondary (confining) compressive stress, a, b and n are three constraints.

Figs. 6–8 show the represented M_r surfaces in terms of the axial stress, σ_1, and confining stress, σ_3 (and σ_2), for the uni- and triaxial tests done in this study, the relative error of the characteristic modelling at the measurement points. It can be clearly seen that, in general, Eq. (3) well represents the resilient modulus of all these mixes under coupled thermal and complex stressed conditions. The relatively big error for the 2nd series data ($\sigma_1 = 20$ & $\sigma_3 = 0$) might be due to that they are from anther study. It can be seen that, at a certain temperature, M_r decreases with the axial stress, σ_1, but increases with the confining stress, σ_3, and meanwhile the confining stress has much more influence than the loading stress, σ_1. Fig. 9 displays the variation of the parametric values of Eq. (3), determined by the fitting results of the Figs. 6–8, with temperature. Setting a as a constant against the temperature, the variation of other two parameters, b and n, against temperature can be reasonably represented using linear trend for simplicity to reduce the potential high nonlinearity brought into the final numerical modelling. Table 3 lists out

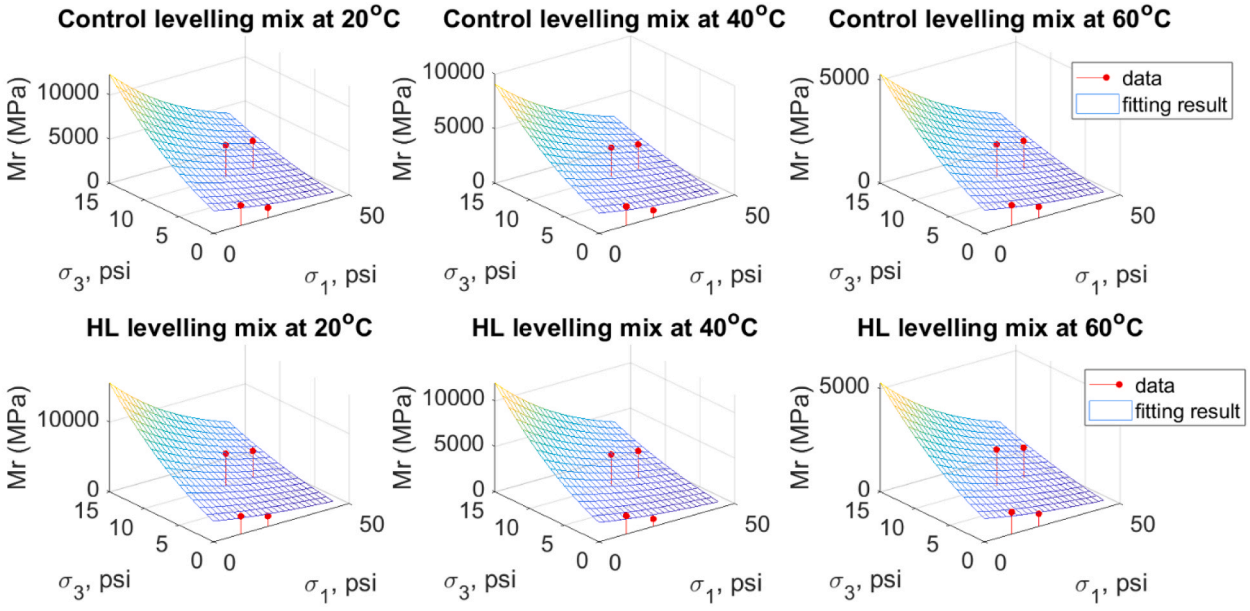

(a) The represented Mr characteristic surface

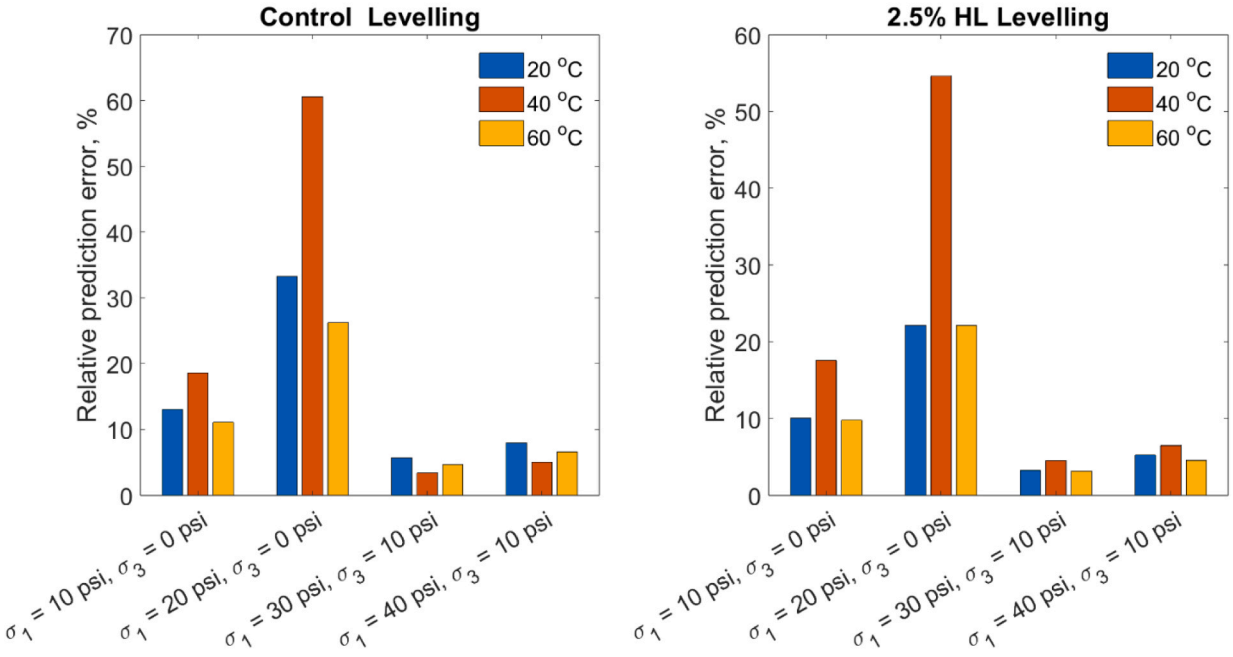

(b) The modelling relative error at the measurement points

Fig. 7. Modelling results of Eq. (3) for the Levelling mixes.

the determined value of the parameter, *a*, and linear models for temperature effect on the parameters, *b* and *n*.

4.2. Permanent deformation, ε_p

For permanent deformation, the Francken model for the ε_p-N curve representation has the advantage to reveal the flow number. However, for engineering practice, the flow number has less concern as asphalt mixes and the constructed pavement have the capacity of tolerance for deformation and distress So it does not mean that the pavement is going to fail to work beyond the Fn. For the reason, power function, i.e, the 1st term of the Francken model, is also commonly employed alone to represent the ε_p-N curve for deformation prediction. Using the form of power function can reduce the complexity for the sake of simple use in practice. So, this paper in the next will adopt the power function form to represent ε_p-N relationship, i.e.: $\varepsilon_p = aN^b$. Fig. 10 shows the fitting result using the function, $\varepsilon_p = aN^b$, for the experimental measurements in the Fig. 2. It can be seen that, although the power function term alone does not clearly reflect the flow number, *Fn*, it well represents the ε_p-N curve in the effective range before the load repetition reaches the flow number when the mixes are assumed to fail but in fact the constructed pavement can continue working. Fig. 11 compares the influences of temperature,

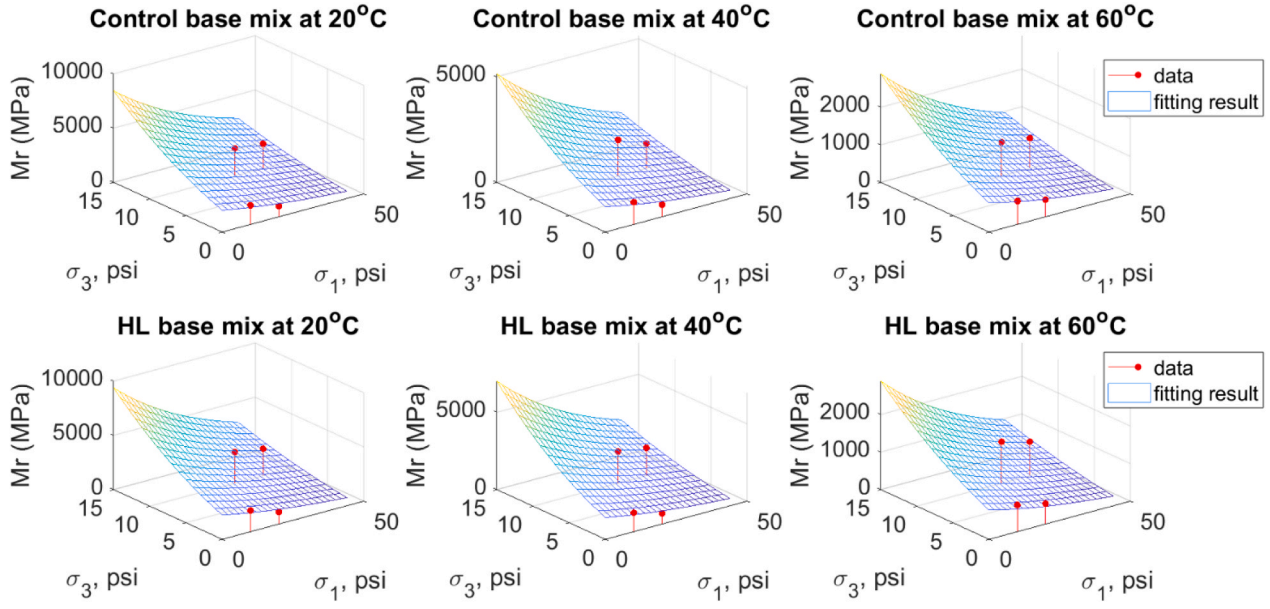

(a) The represented Mr characteristic surface

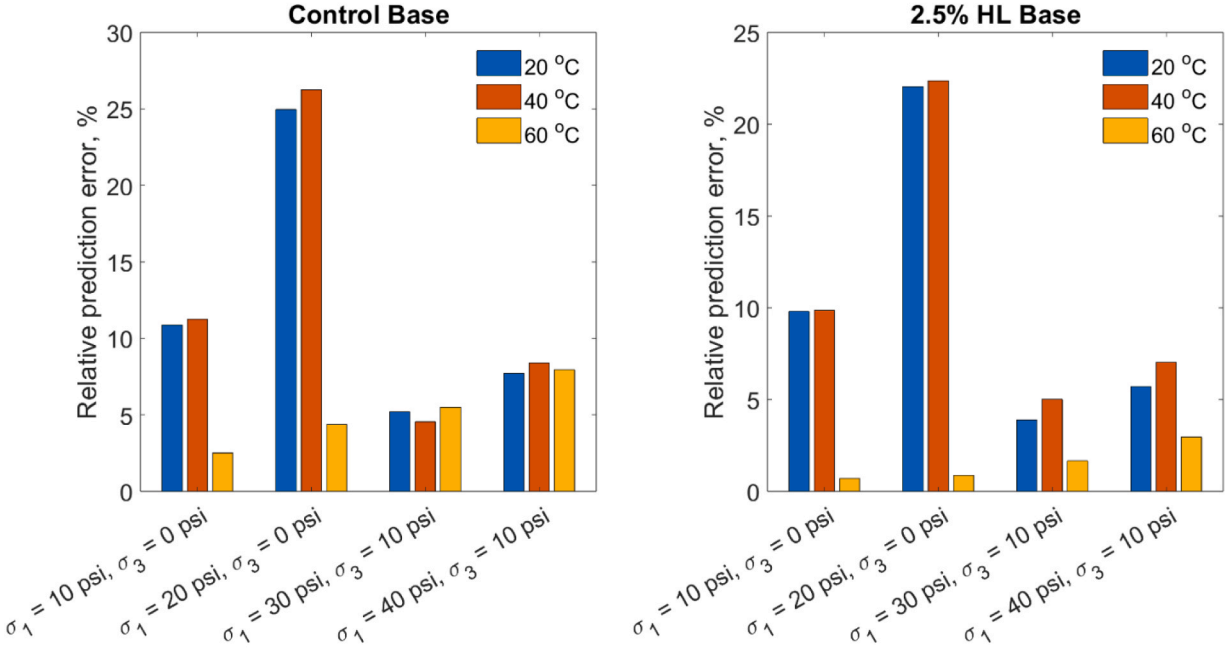

(b) The modelling relative error at the measurement points

Fig. 8. Modelling results of Eq. (3) for the Base mixes.

stress state and types of mix, and the effect of HL on the two parameters, *a* and *b*.

Comparing the Fig. 11 with the Fig. 5, it can be seen that the variation trends of the parameters, *a* and *b*, of the power function model against stress states at different temperature present a similarity as that of the resilient modulus, M_r. The axial load stress and the confining stress have similarly showed an opposite effect on the two parameters. However, in general, they display a positive correlation with the axial stress, σ_1, but a negative correlation with the confining stress, σ_1. A trend just opposites that of the M_r. Based on the observation, this paper proposes to use a revised form of Eq. (2) to characterize the stress state effect on the permanent deformation through the two parameters, i.e.:

$$[a, b] = \sigma_1^m(\sigma_3 + k)^n \tag{4}$$

where *a* and *b* are the parameters of the power function for ε_p-N curves, *m*, *n*, and *k* ate the three new constants of the model for the ε_p characterisation application. The proposed Eq. (4) is applicable for both uni- and tri-axial stress states.

Figs. 12 and 13 show the represented parametric surfaces of the two determined parameters, *a* and *b*, of the power function model fitted to the ε_p-N curves for the control and HL mixes. The markers of 'data' and 'fitting result' compare visually the determined values of the

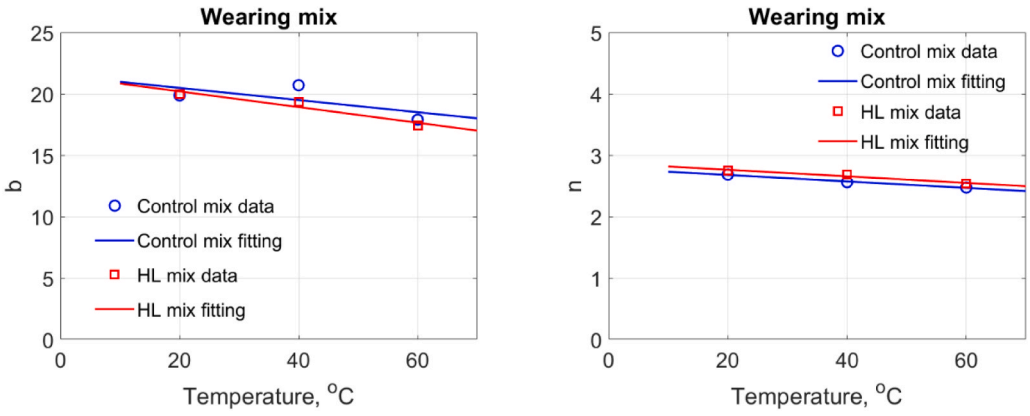

(a) Wearing mix

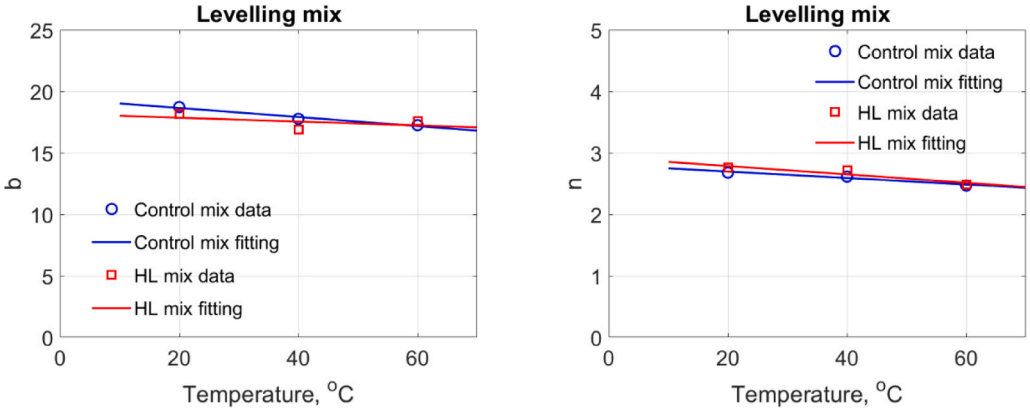

(b) Levelling mix

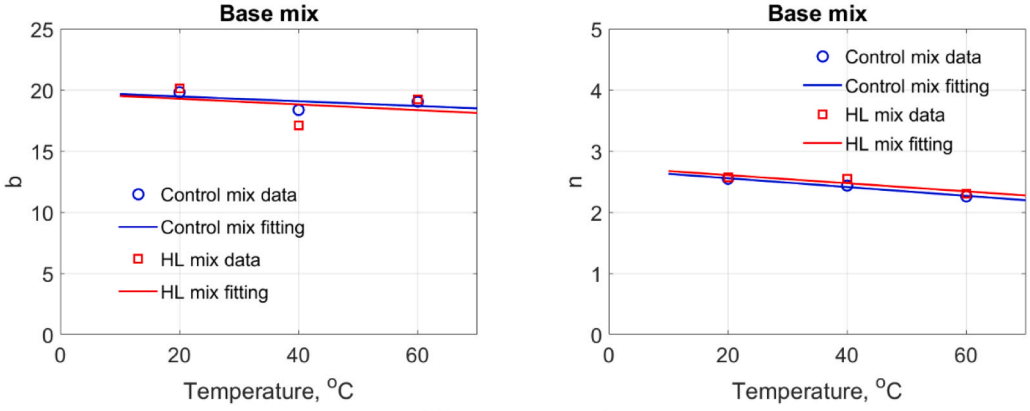

(c) Base mix

Fig. 9. Parametric variation of Eq. (3) with temperature.

Table 3
The parametric variation of the Eq. (3) against temperature.

Control mixes			
	Wearing	Levelling	Base
a	– 0.025		
b	– 4.95e-2 T + 21.47	– 3.68e-2 T + 19.38	– 1.95e-2 T + 19.86
n	– 5.25e-3 T + 2.783	– 5.25e-3 T + 2.8	– 7.2e-3 T + 2.7
HL mixes			
	Wearing	Levelling	Base
a	– 0.025		
b	– 6.38e-2 T + 21.47	– 1.55e-2 T + 18.16	– 2.33e-2 T + 19.75
n	– 5.35e-3 T + 2.87	– 6.78e-3 T + 2.92	– 6.65e-3 T + 2.74

parameters, *a* and *b*, from the ε_p-N results in Fig. 10 with the values on the parametric fitting surfaces. The naked eye direct comparison clearly demonstrates that the parametric model, Eq. (4), and the power function together can well represent the permanent deformation of all these mixes under both uni- and tri-axial stress states when exposed to different temperature conditions. Fig. 14 shows the variation of the parametric model's parameters, *m*, *k* and *n*, with temperature. For the wearing mixes, the one with HL modification generally has much less variation of the *m*, *k*, and *n* with temperature. It indicates that HL helps the wearing layer on the thermal deformation resistance. This attribute remains for the levelling mixes but not for the base mixes. For the base mixes there is little comparable trend for the variation of the *m*, *k* and *n*

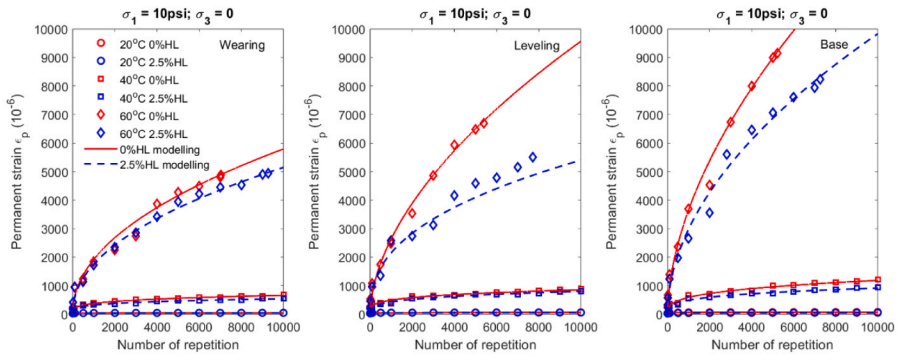

(a) Axial stress (σ_1) is 10 psi (68.9 kPa), confining stress (σ_3) is 0

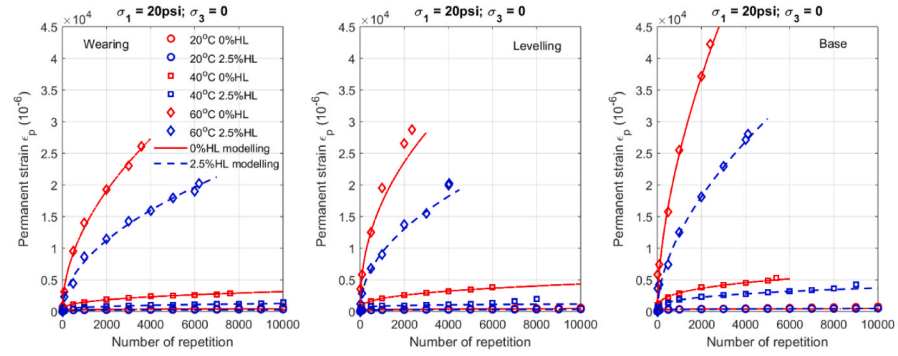

(b) Axial stress (σ_1) is 20 psi (137.9 kPa), confining stress (σ_3) is 0

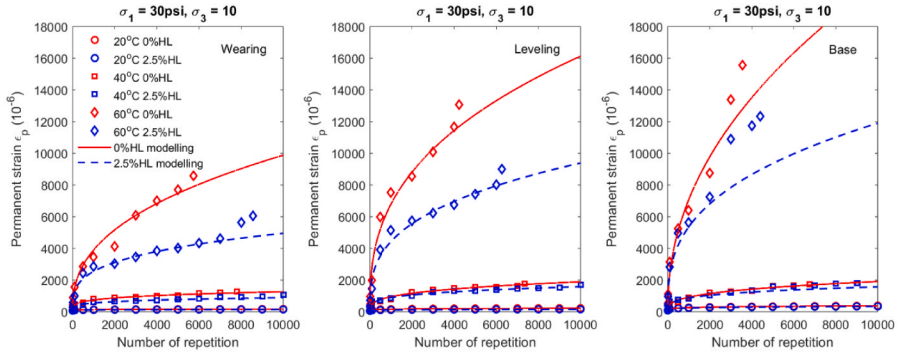

(c) Axial stress (σ_1) is 30 psi (206.9 kPa), confining stress (σ_3) is 10 psi (68.9 kPa)

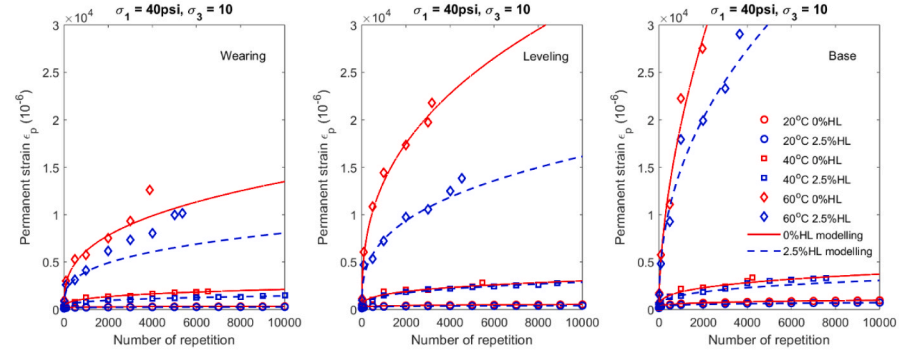

(d) Axial stress (σ_1) is 40 psi (275.8 kPa), confining stress (σ_3) is 10 psi (68.9 kPa)

Fig. 10. The represented permanent deformation by the power function model.

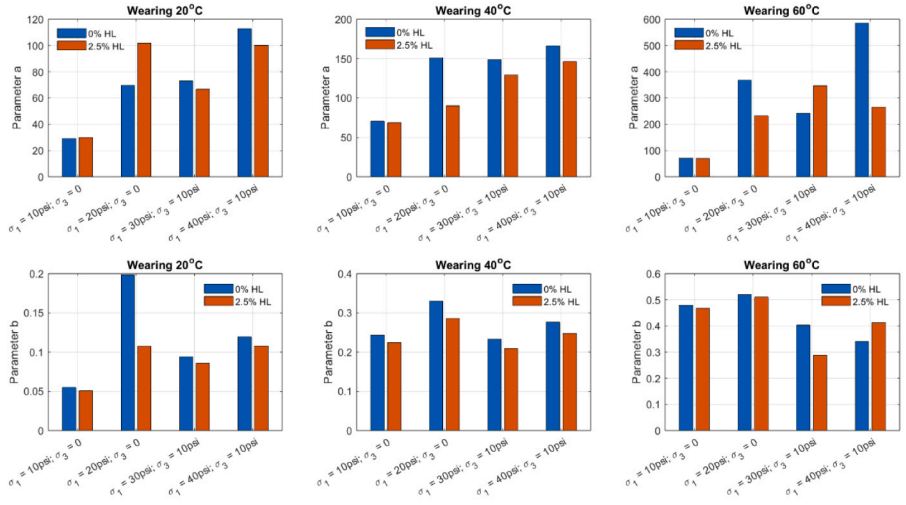

(a) Wearing mixes

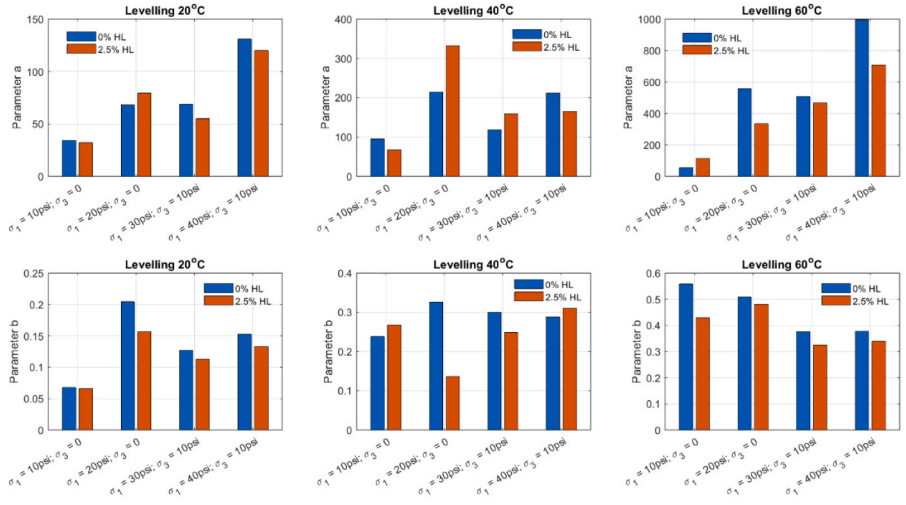

(b) Levelling mixes

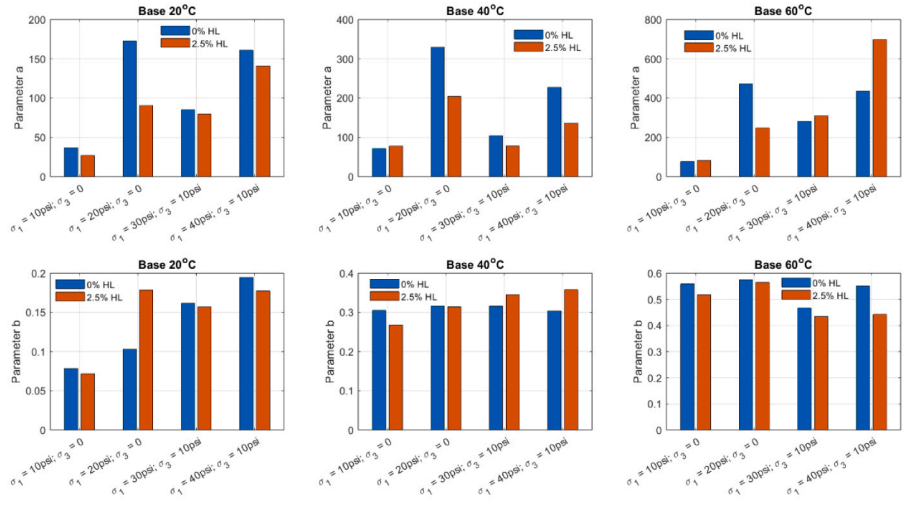

(c) Base mixes

Fig. 11. The determined power function parameters, *a* and *b*, for the modelling in Fig. 2.

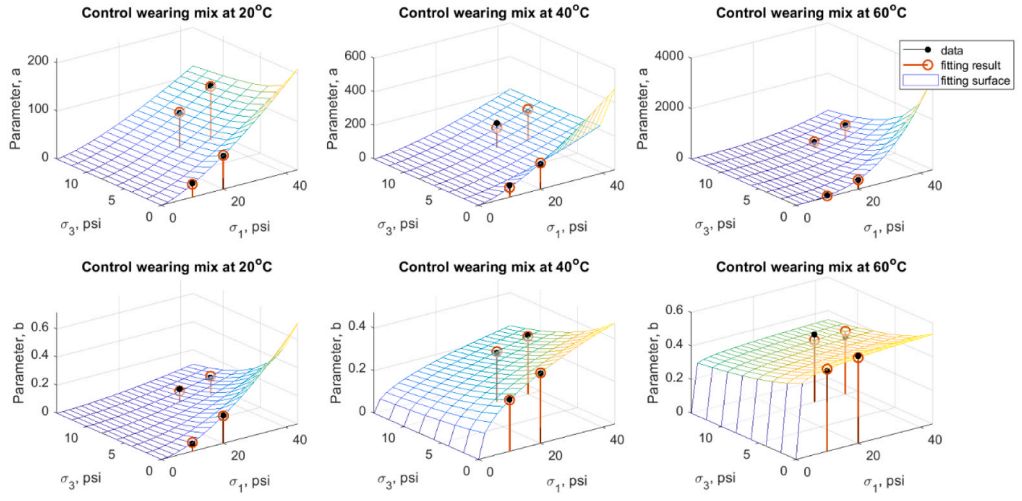

(a) Wearing mix

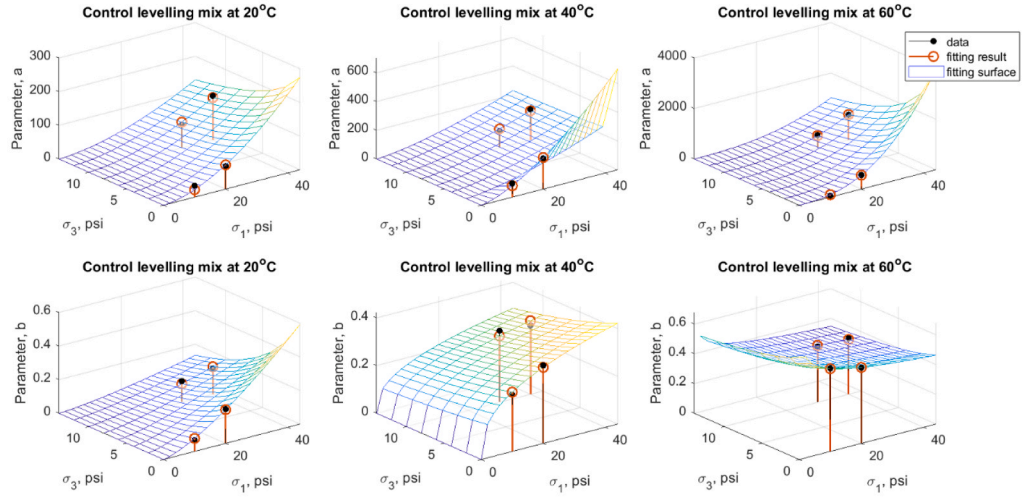

(b) Levelling mix

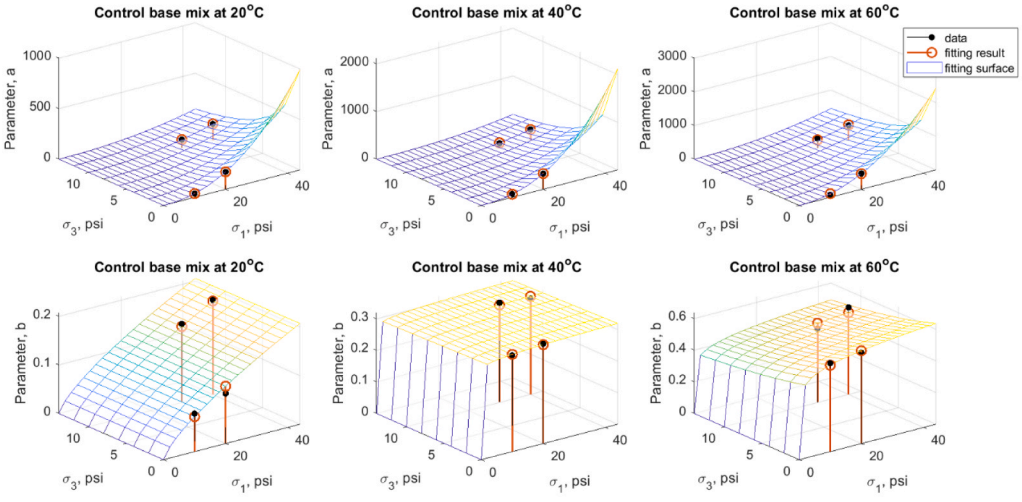

(c) Base mix

Fig. 12. The representative characteristic surface using Eq.(4) for the parameters, *a* and *b*, of the ε_p-N power function modeling result (as demonstrated in Fig. 10) in the case of control mixes.

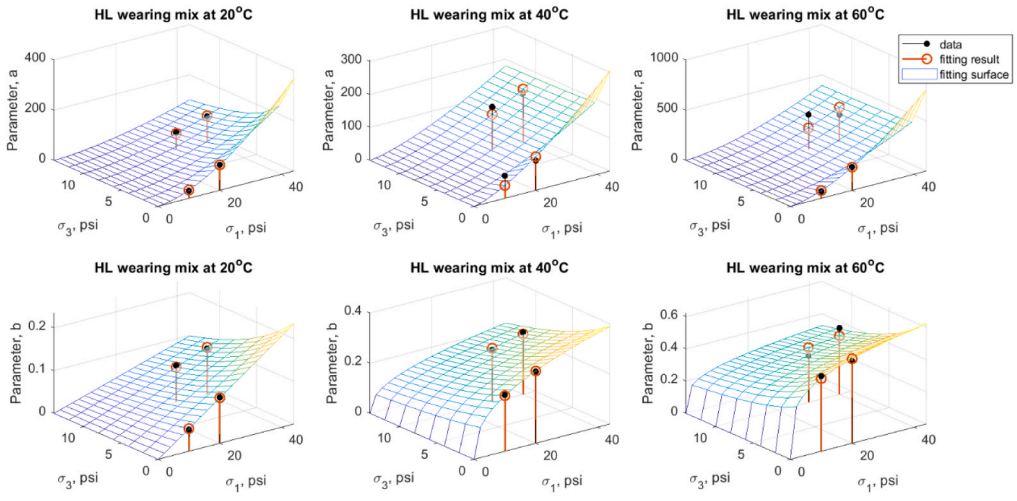

(a) Wearing mix

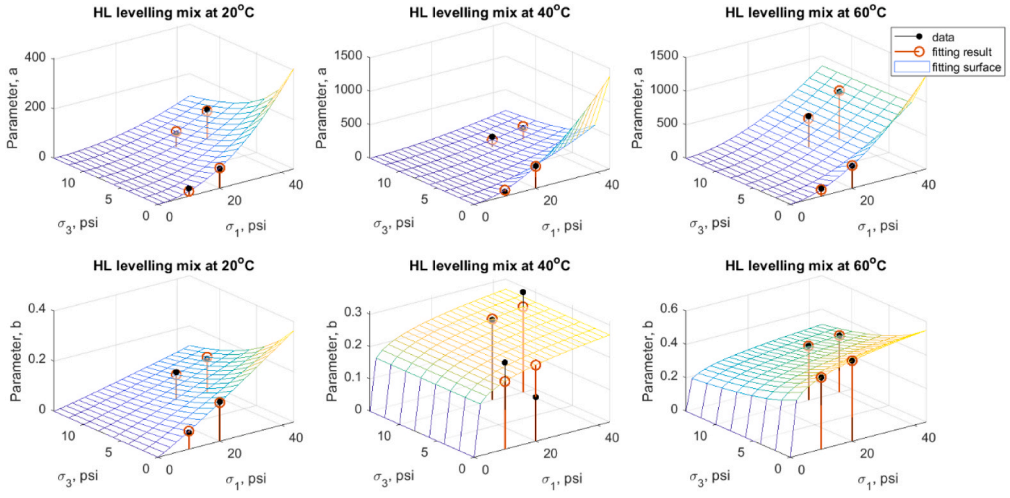

(b) Levelling mix

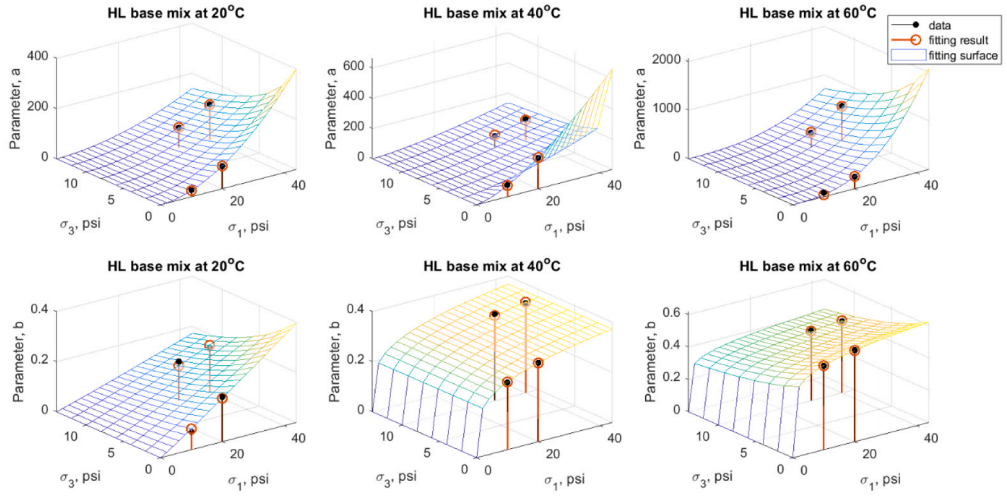

(c) Base mix

Fig. 13. Francken's parametric characteristic surface, Eq.(4), for the 2.5% HL mixes.

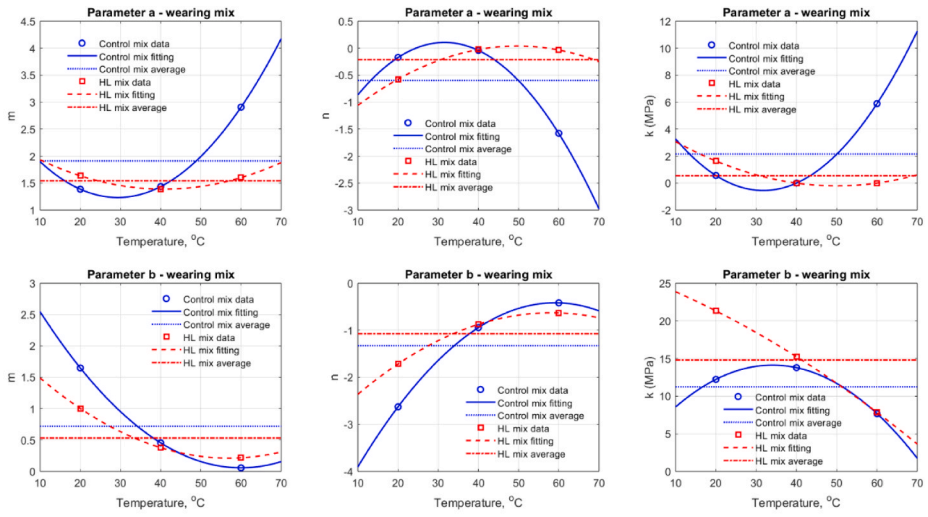

(a) Wearing mixes

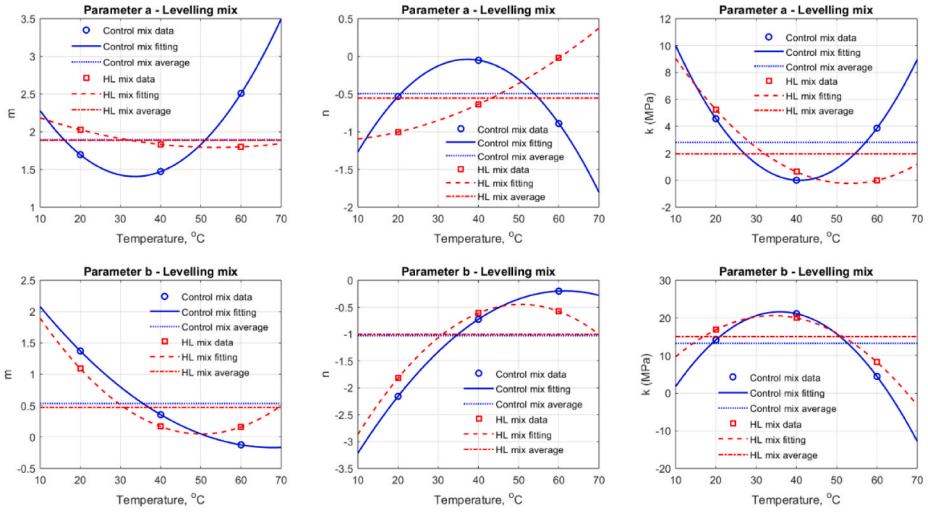

(b) Levelling mixes

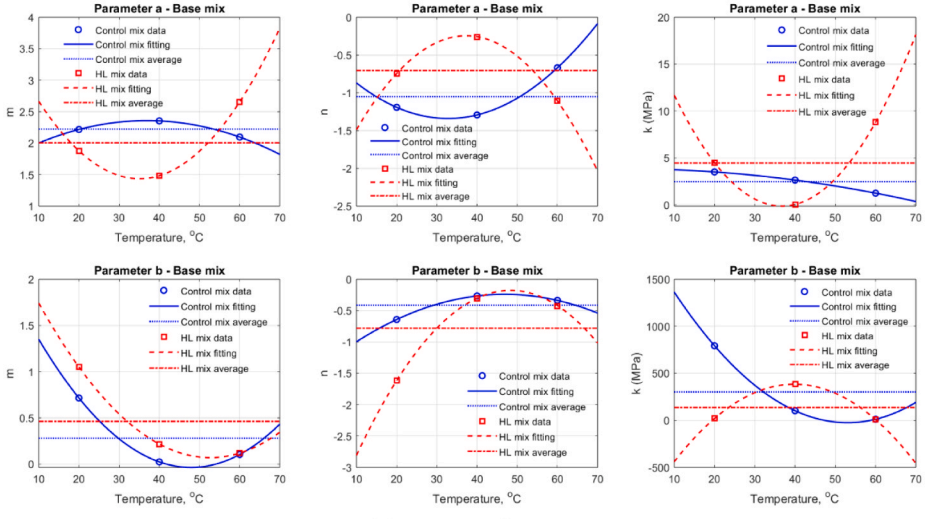

(c) Base mixes

Fig. 14. The representative characteristic surface using Eq.(4) for the parameters, *a* and *b*, of the ε_p-N power function modeling result (as demonstrated in Fig. 10) in the case of HL modified mixes.

Table 4
The determined Eq. (4) for the Franken parameter against temperature.

Eq. (4) **parameter, a**			
	Control Wearing	Control Levelling	Control Base
m	1.78e+ 3 T^2 – 1.04e-1 T + 2.76	1.58e-3 T^2 – 1.06e-1 T + 3.18	–4.91e-4 T^2 + 3.63e-2 T + 1.69
n	-2.09e-3 T^2 + 1.32 T - 1.97	-1.65e-3 T^2 + 1.23e-1 T - 2.33	9.07e-4 T^2 – 5.95e-2 T - 0.37
k	8.08e-3 T^2 – 5.13e-1 T + 7.6	1.06e-2 T^2 – 8.61e-1 T + 17.57	-6.56e-4 T^2 – 4.13e-3 T + 3.85
	HL Wearing	HL Levelling	HL Base
m	5.75e-4 T^2 – 4.69e-2 T + 2.34	2.01e-4 T^2 – 2.18e-2 T + 2.38	1.96e-3 T^2 – 1.37e-1 T + 3.84
n	-6.99e-4 T^2 + 6.95e-2 T - 1.68	3.06e-4 T^2 + 6.65e-5 T - 1.13	-1.67e-3 T^2 + 1.25e-1 T - 2.57
k	2.05e-3 T^2 – 2.05e-1 T + 4.92	4.99e-3 T^2 – 0.5305 T + 13.86	1.66e-2 T^2 – 1.22 T + 22.21
Eq. (4) **parameter, *b***			
	Control Wearing	Control Levelling	Control Base
m	9.95e-4 T^2 – 1.19e-1 T + 3.64	6.67e-4 T^2 – 9.08e-2 T + 2.92	9.64e-4 T^2 – 9.24e-2 T + 2.18
n	-1.45e-3 T^2 + 1.71e-1 T - 5.47	-1.14e-3 T^2 + 1.4e-1 T - 4.5	-5.57e-4 T^2 + 5.22e-2 T - 1.46
k	-9.59e-3 T^2 + 6.53e-1 T + 3.0	-2.96e-2 T^2 + 2.13 T - 16.54	7.5e-1 T^2 – 79.5 T + 2084
	HL Wearing	HL Levelling	HL Base
m	5.79e-4 T^2 – 6.6e-2 T + 2.09	1.15e-3 T^2 – 1.15e-1 T + 2.93	9.18e-4 T^2 – 9.68e-2 T + 2.62
n	-7.48e-4 T^2 + 8.69e-2 T - 3.15	-1.47e-3 T^2 + 1.49e-1 T - 4.21	-1.79e-3 T^2 – 1.73e-1 T - 4.36
k	-1.66e-3 T^2 – 2.04e-1 T + 26.08	-1.86e-2 T^2 + 1.28 T - 1.23	-9.25e-1 T^2 + 73.67 T - 1083

between the HL mixes and the control mix. This could be explained by the low total mineral additive content and high air void content (Table 1) of the base mixes. The temperature effect on the ε_p is further characterised using parabolic function to represent the variation of the parameters, *m*, *k* and *n,* against temperature. All the determined parabolic functions are listed out in Table 4.

5. Modelling case study of pavement rutting prediction

Using the material property characteristic models, the Eqs. (3) and (4), a numerical modelling was conducted to compare the rutting resistance of pavement constructed using HL modified asphalt concrete mixes with the that using the control ones. A finite element model for a single lane pavement created before [34] was adopted. The mechanical and thermal boundary conditions are illustrated in Fig. 15 in half for a symmetric pavement structure. A static vertical pressure of 1000 kg was applied as the assumed equivalent traffic load (Fig. 15(a)). The case is set for a region in the north-west of England in the UK. The annual daily temperature information (Fig. 15(b)) was referred to a survey reported [35]. The daily variation of temperature in 10 °C is also considered as illustrated in Fig. 15(c). .

As the traffic load is in the form of a static load, the case study only investigated the annual climatic temperature variation effect on the permanent deformation (rutting). The thermal properties of these concrete mixes had been reported before [34]. In this study, the coupled thermomechanical situation has excluded the thermal expansion and contraction factors of all materials themselves as their values are very small and meanwhile incorporating them in the model introduces in high nonlinearity which presented a challenge for the FEA solver, COMSOL Multiphysics, that we used. On the other hand, as rutting primarily happens under the traffic loading, the discussion on rutting is focused on the deformation along the vertical line under the inside of the traffic load (Wheels), the point A in Fig. 15(a).

Fig. 16 shows the results of the principal stresses, which is defined by the Eq. (5), and the shear stress.

$$\sigma_{p1} = \frac{1}{2}(\sigma_x + \sigma_y) + \sqrt{\tau_{xy}^2 + \frac{1}{4}(\sigma_x - \sigma_y)^2} \tag{5a}$$

$$\sigma_{p1} = \frac{1}{2}(\sigma_x + \sigma_y) - \sqrt{\tau_{xy}^2 + \frac{1}{4}(\sigma_x - \sigma_y)^2} \tag{5b}$$

Fig. 16(a)-(b) indicates that the asphalt layers are mostly under tensile in both the 1st and 2nd principal stress directions, but in compression at the position directly under the traffic load. The maximum tensile stress happens in the base layer at the interface with the subbase. Fig. 16(c) shows the shear stress in x-y plane. It indicates that the maximum shear stress happens in the region of the levelling layer and at the position under the traffic load, where it has different direction at the two edge sides of the traffic load (wheels). The modelling simulation implies that the most vulnerable place exposed for potential fatigue cracking is at the bottom of the base layer while the most vulnerable place exposed for potential rutting is the levelling layer and directly below the traffic load.

Fig. 17 shows the FE modelling results of the resilient deformation along the vertical line under the position A. It can be seen that in the layers of levelling and base the local x displacement changes have the relatively big variation in different climatic seasons (in the modelling a reference temperature 10 °C was assumed to estimate the thermal stress). The modelling time of 720 hrs occurred in February, 2880 hrs in May, 5040 hrs in August, and 7200 hrs in November. For the vertical displacement, the top surface layer shows the most climatic seasonal variation. The temperature effect on the vertical displacement reduces with the pavement depth.

Fig. 18 shows the thermal stress in the asphalt and subbase layers under the position A. It can be seen that climatic seasonal temperature change has significant effect on the thermal stress in the asphalt layers. The thermal stress in spring (2880 h) and autumn (7200 h) is relatively small. However, the thermal stress changes from compression in winter (720 h) to tensile in summer (5040 h). The thermal stress in subbase is neglectable. Such climatic variation of thermal stress plays a key role for thermal fatigue as discussed in a previous study [Al Ashaibi et al., 2022].

Fig. 19 shows the mechanical shear strain under the position A due to traffic load. It can be seen that the mechanical shear strain also shows variation in different seasons because of the temperature effect on material properties, such as the resilient modulus. However, in comparison with the Fig. 18, the seasonal variation of the mechanical shear strain is much less than that of the thermal stress.

Fig. 20 compares the vertical displacement under position A between the pavements constructed using the control mixes, HL = 0%, and the modified ones, HL = 2.5%. It can be seen that the pavement using HL modified mixes has less vertical displacement in all four different seasons.

Fig. 21 compares the shear strain under position A between the pavements constructed using the control mixes, HL = 0%, and the modified ones, HL = 2.5%. It displaces that, in line with the results in Fig. 20 the pavement using HL modified mixes has less shear strain in all four different seasons as well.

Fig. 22 compares the thermal strain under position A between the pavements constructed using the control mixes, HL = 0%, and the modified ones, HL = 2.5%. The results show that the pavement using HL modified mixes has bigger thermal strain in tensile in summer season (5040 hrs), but has less thermal strain in compression in all other three seasons. The results implies that the HL modification might be more beneficial for pavement construction in relatively cold geo-region.

As the modelling didn't consider the loading repetition of traffic, no demonstration of the permanent deformation, ε_p, prediction using the model Eq. (4) has been performed in this paper. A demonstration for this application will be reported in another paper. The numerical simulation so far has demonstrated that the pavement deformation is subjected to both the complex triaxial stress situation and the climatic temperature

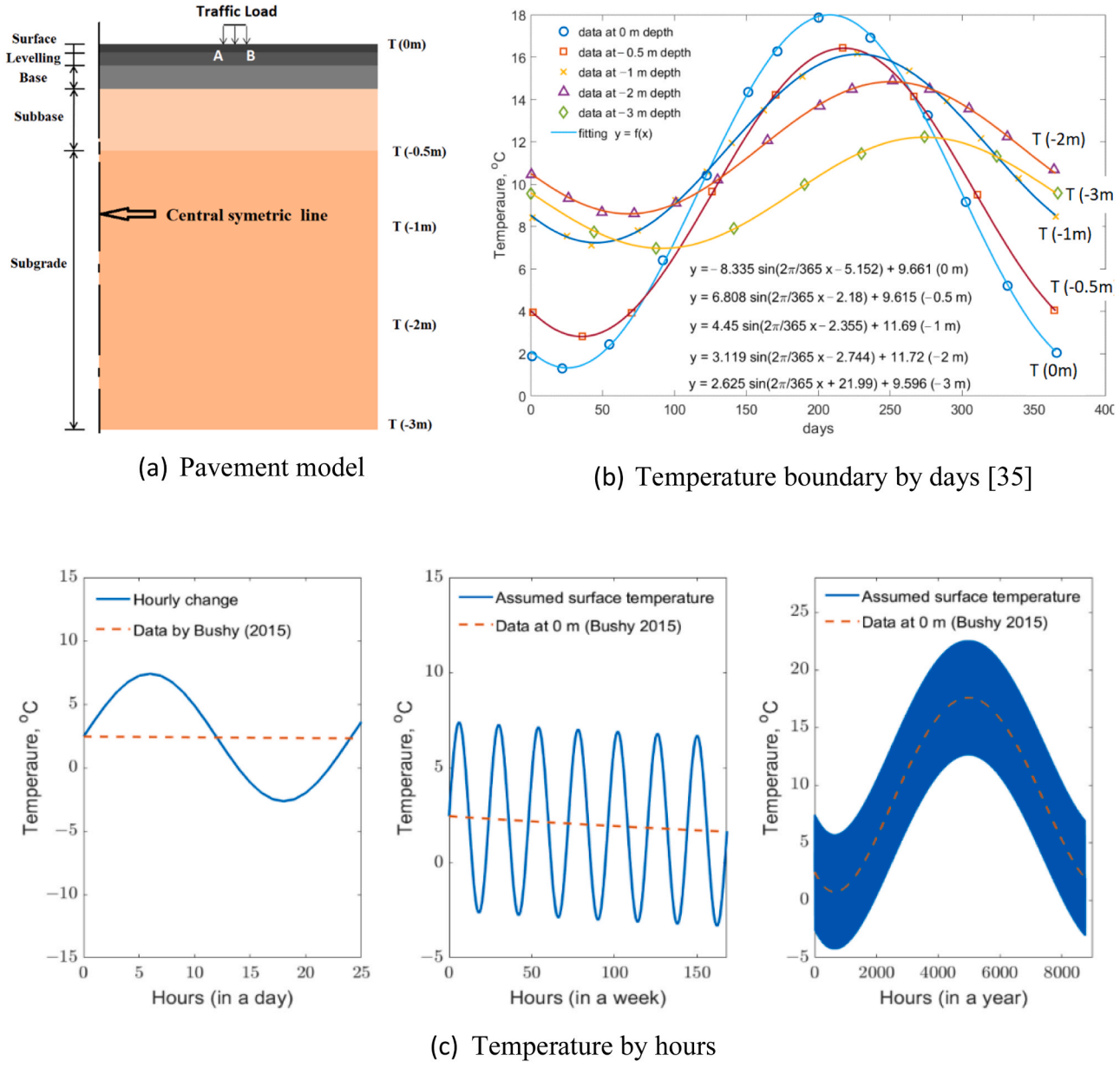

Fig. 15. Pavement case study modelling (in reference to Al-Ashaibi et al. [34]).

Table 5
Finite element geometric data.

	Surface/ Wearing	Binder/ Levelling	Base	Subbase	Subgrade	Traffic load / Wheel
Thickness (mm)	50	70	90	300	2500	-
Width (mm)	1800					25

condition. The proposed characteristic models for the material properties not only produce good representation but also effectively work well when adopted in the numerical simulation.

6. Conclusion

This paper reports research on uni- and tri-axial tests for the permanent deformation and resilient modulus of hydrated lime modified HMA concrete mixes at different temperature conditions, and comparison with the control mixes with no use of HL. Based on the experimental results, a unified mathematical model has been proposed to characterize the dependence of the resilient modulus and permanent deformation on complex stress condition and temperature states of mixes. Together with a modelling case study, the following conclusions can be drawn from this study.

- HL additive helps the deformation resistance of the HMA concrete. Its effect is particularly pronounced when mixes have high content of the total mineral filler, and accordingly high HL content.

- The elastic resilient modulus for fresh HMA displays initial increase when exposed to repetitive loads. This is probably due to aggregate re-arrangement in the asphalt matrix which improves the mix of asphalt paste and aggregates. This explanation is in line with the results that the HL addition reduces the resilient strain of mixes, particularly at higher temperature because HL improves the stiffness of the asphalt paste.

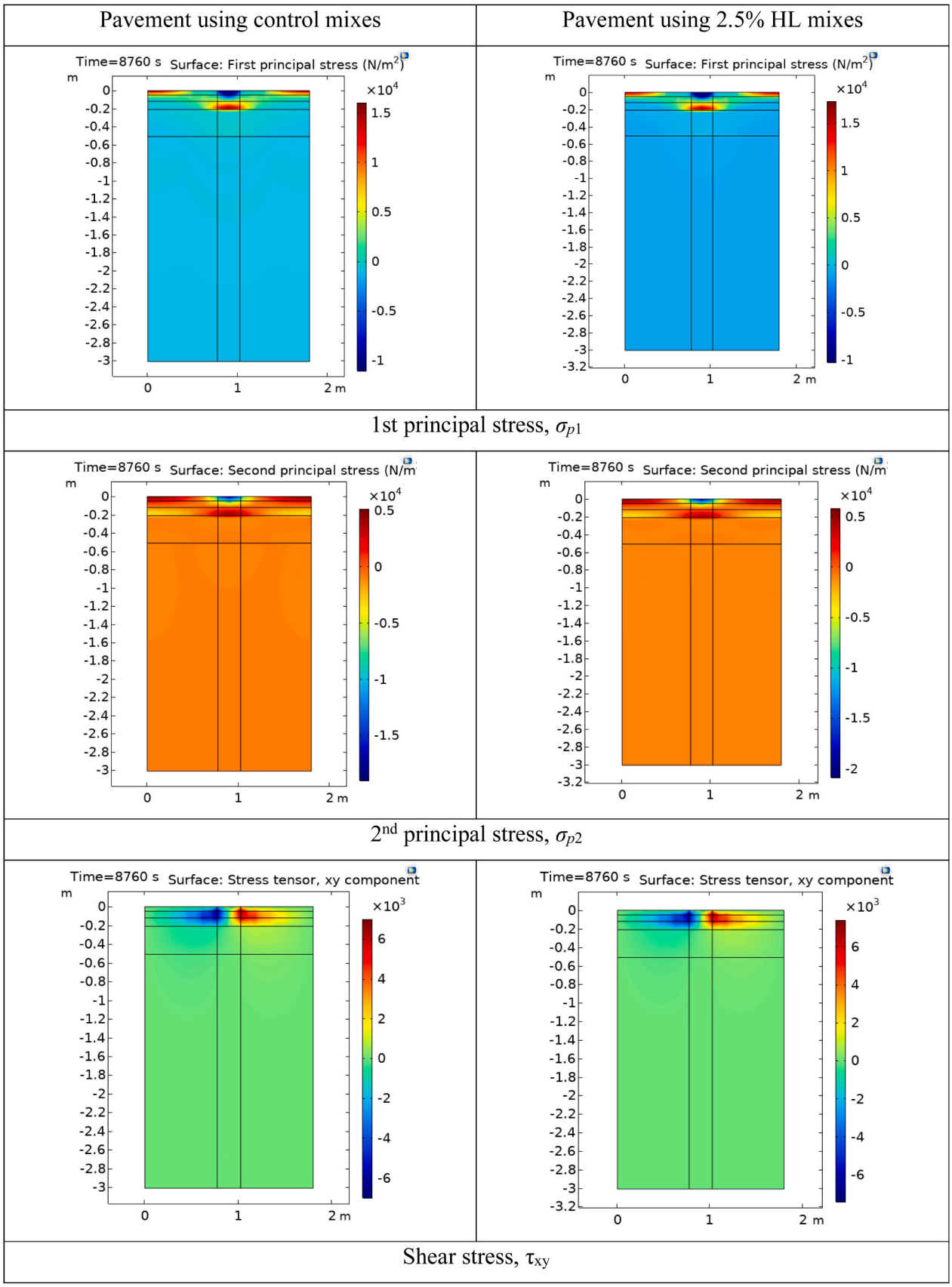

Fig. 16. The FE modelling results of the mechanical principal and shear stresses distribution.

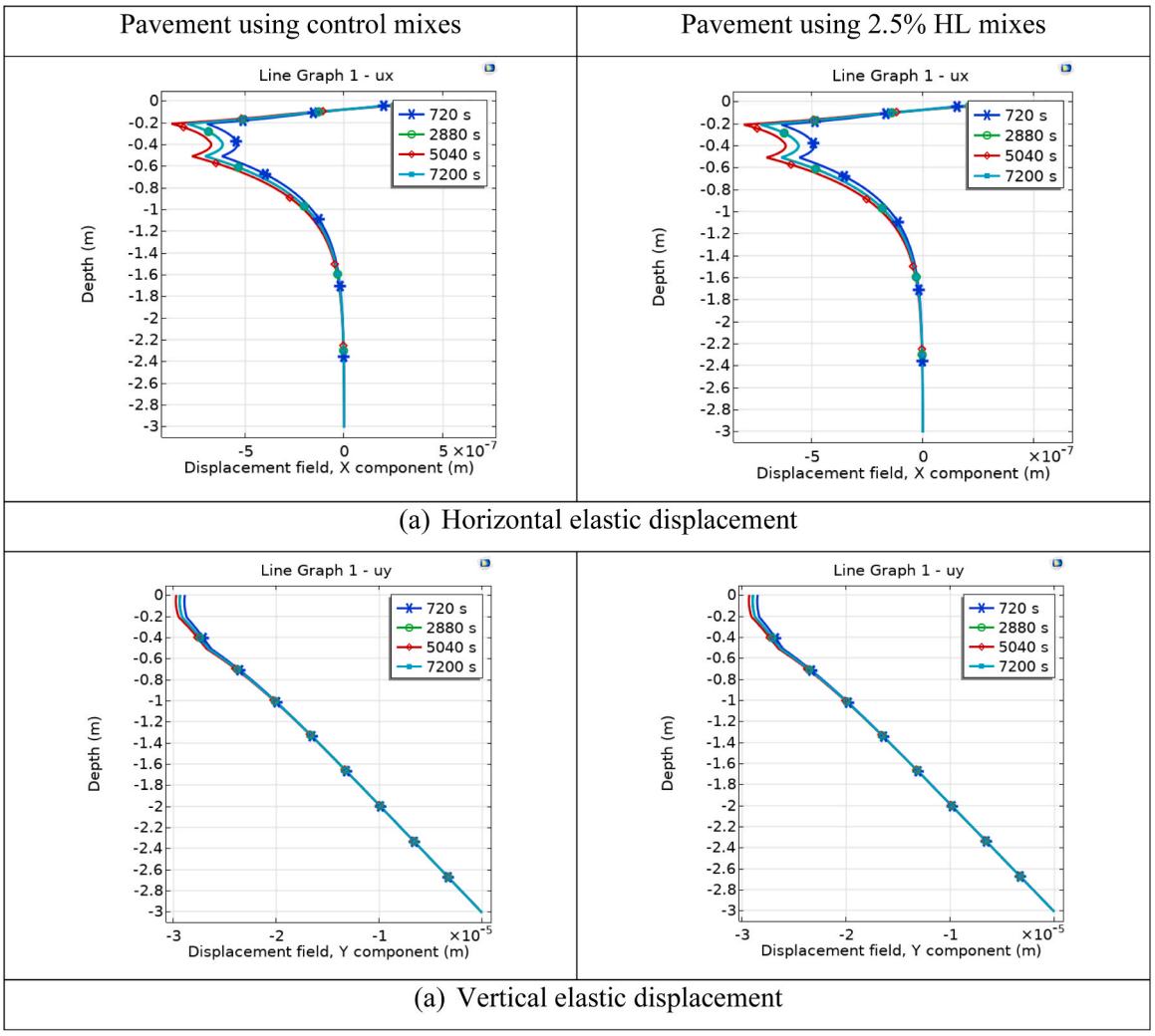

Fig. 17. The FE modelling results of the resilient deformation under position A.

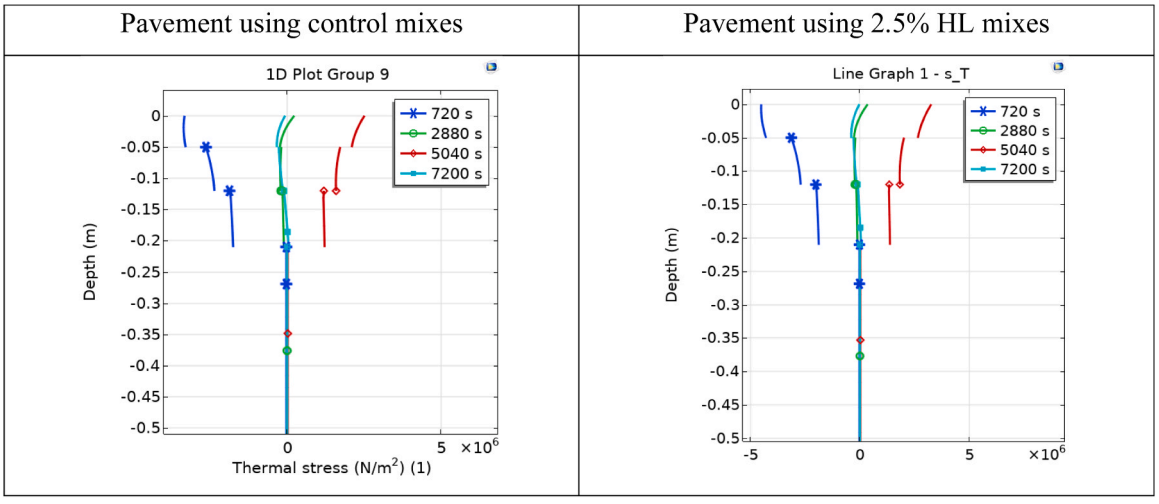

Fig. 18. Thermal stress in asphalt layers and the subbase under position A.

- Francken model can provide an effective representation for the material property, the permanent deformation curve against load repetition under complex stress conditions, and well identify the flow number. However, a simplified power function works well enough for the effective part of ε_p-N curves before material failure.
- The proposed unified characteristic model for the resilient modulus and the parameters of the power function model for the ε_p-N curves

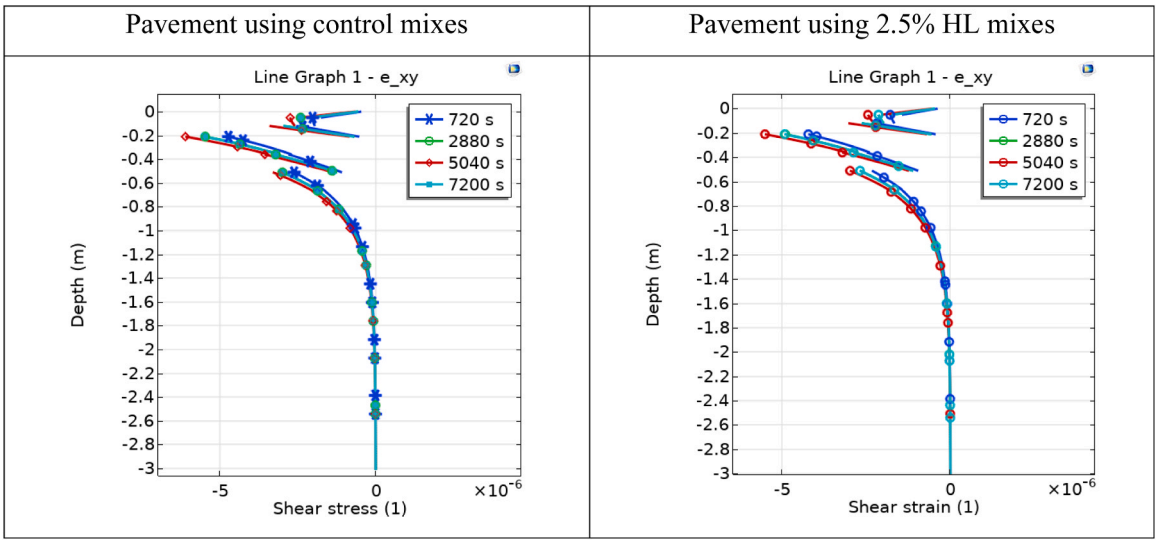

Fig. 19. The vertical shear strain under position A.

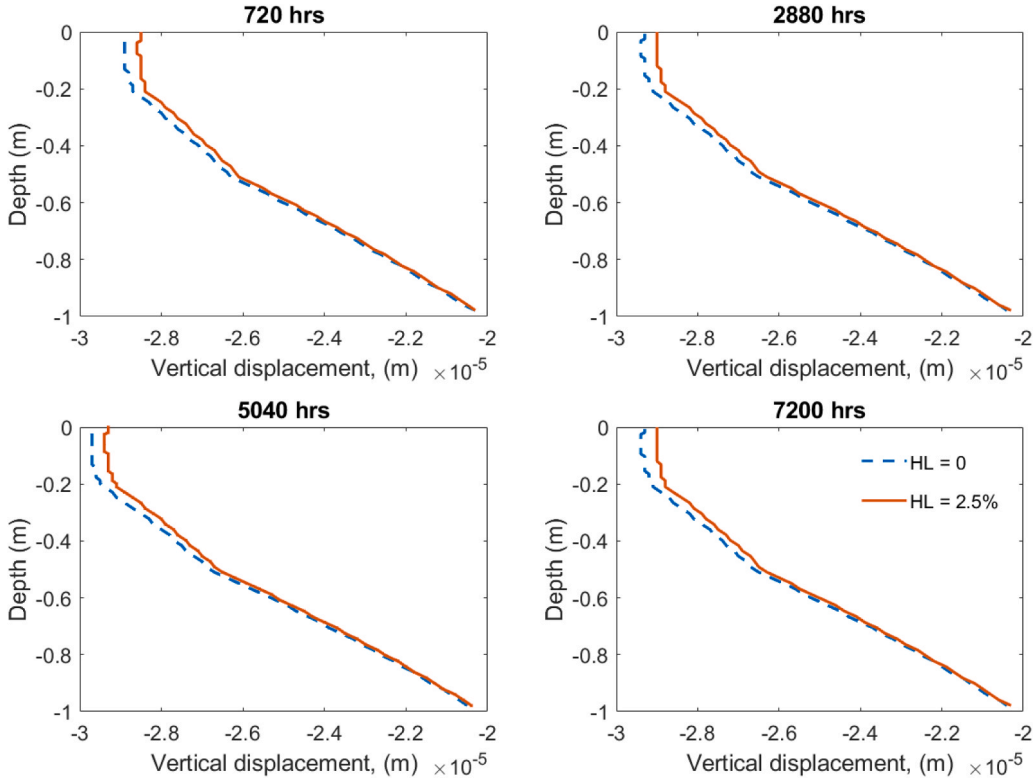

Fig. 20. Comparison of the vertical displacement under A between the HL0 and HL2.5 pavements.

give good representation for the two material properties under complex conditions from uniaxial to triaxial stress states at different temperature.

- The parametric variation of the unified characteristic model well reflects the HL effect of the improvement on HMA concrete rutting resistance. The proposed characteristic model can be implemented into numerical modelling and simulation for pavement structural analysis, deformation and rutting prediction when pavement is exposed to coupled thermomechanical loading in service.
- The numerical case study demonstrated the benefit of the HL modified asphalt mixes for the constructed pavement in terms of the thermal fatigue and thermomechanical deformation resistance.

CRediT authorship contribution statement

Al Ashaibi Azedin: Writing – original draft, Funding acquisition. **Haynes Jonathan:** Writing – review & editing, Supervision. **Weekes Laurence:** Writing – review & editing, Supervision. **Albayati Amjad:** Writing – review & editing, Validation, Supervision, Resources, Project administration, Methodology, Investigation, Formal analysis, Data curation, Conceptualization. **Wang Yu:** Writing – review & editing, Writing – original draft, Visualization, Validation, Supervision, Software, Resources, Project administration, Methodology, Investigation, Funding acquisition, Formal analysis, Data curation, Conceptualization.

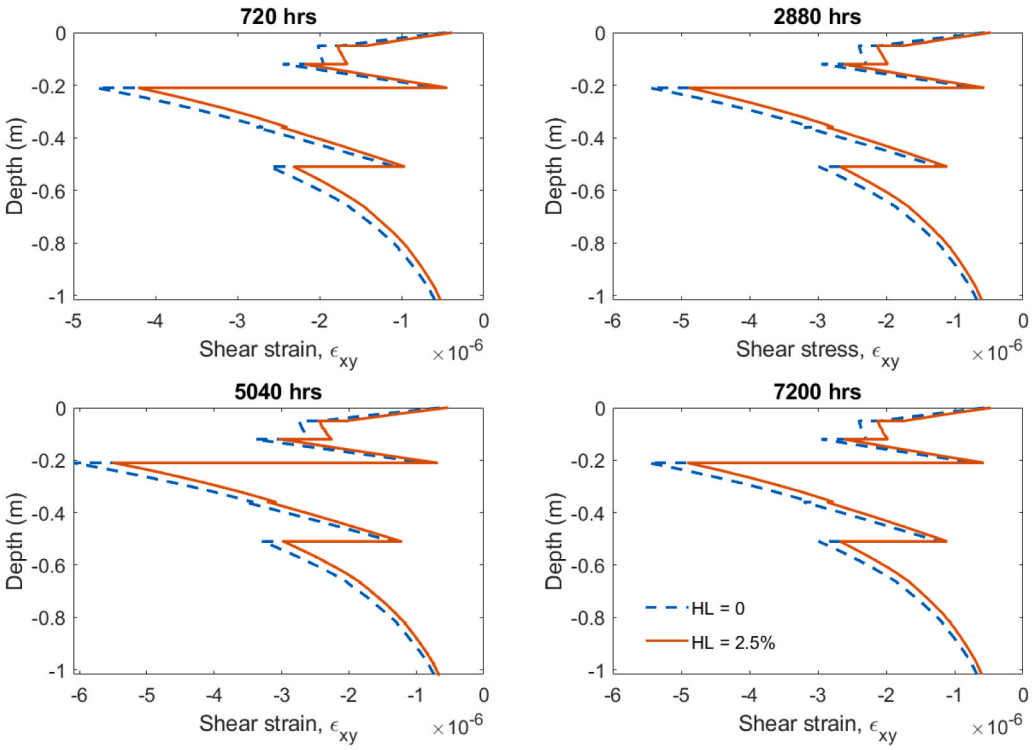

Fig. 21. Comparison of the shear stress under A between the HL0 and HL2.5 pavements.

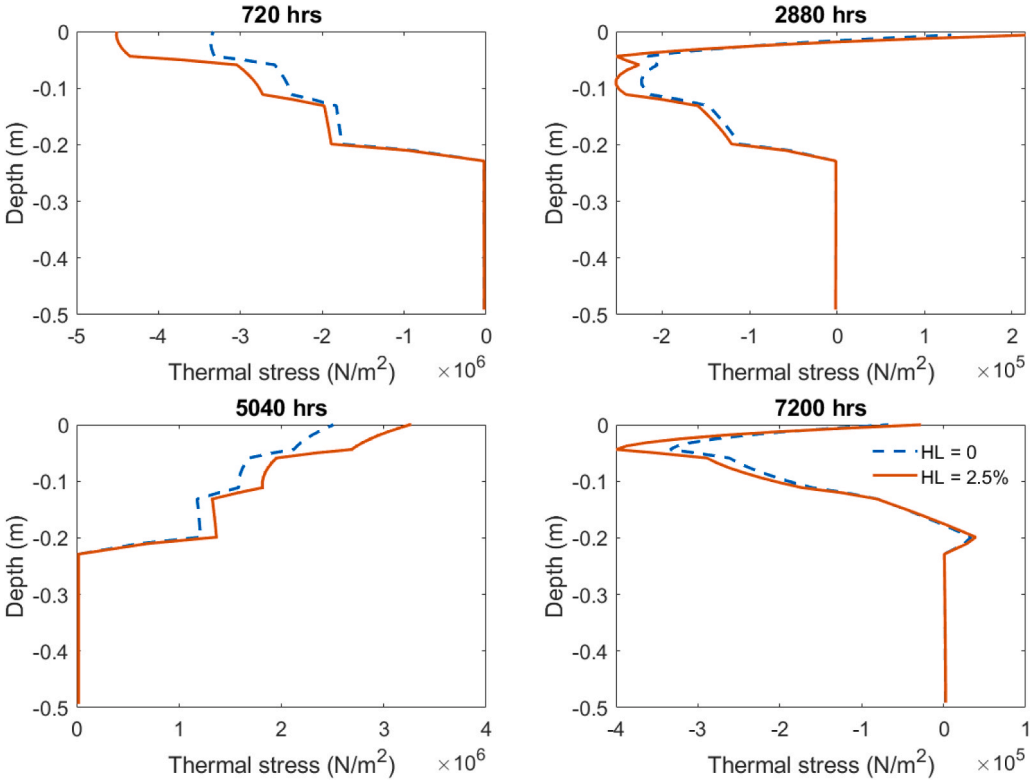

Fig. 22. Comparison of the thermal stress under A between the HL0 and HL2.5 pavements.

Declaration of Competing Interest

The authors declare that they have no known competing financial interests or personal relationships that could have appeared to influence the work reported in this paper.

Data availability

Data will be made available on request.

Acknowledgment

Part of the research is funded by a Ph.D. studentship sponsored by the government of Libya.

Appendix. Extra information of the aggregate and fillers

Table A1 presents the selected aggregate gradation alongside the specification limits for Wearing, Levelling, and Base courses according to the ASTM D 3515. The selected gradations for these courses meet the corresponding specification limits for mix types D-5, D-4, and D-3, respectively. The data includes sieve sizes, ranging from 37.0 mm (1.5 in.) to 0.075 mm (No.200), and the corresponding percent passing for each course.

Table A1
The aggregate gradation against the specification limits.

Sieve Size		Percent Passing (%)					
mm	inch	Wearing Course		Leveling Course		Base Course	
		Selected gradation	Specification limit for mix type D-5, ASTM D3515	Selected gradation	Specification limit for mix type D-4, ASTM D3515	Selected gradation	Specification limit for mix type D-3, ASTM D3515
37.0	1.5					100	100
25.0	1			100	100	95	90-100
19.0	3/4	100	100	95	90-100	83	
12.5	1/2	95	90-100	80		68	56-80
9.5	3/8	83	…	69	56-80	61	…
4.75	No.4	59	44-74	50	35-65	44	29-59
2.36	No.8	37	28-58	35	23-49	32	19-45
0.3	No.50	13	5-21	13	5-19	11	5-17
0.075	No.200	7	2-10	6	2-8	5	1-7

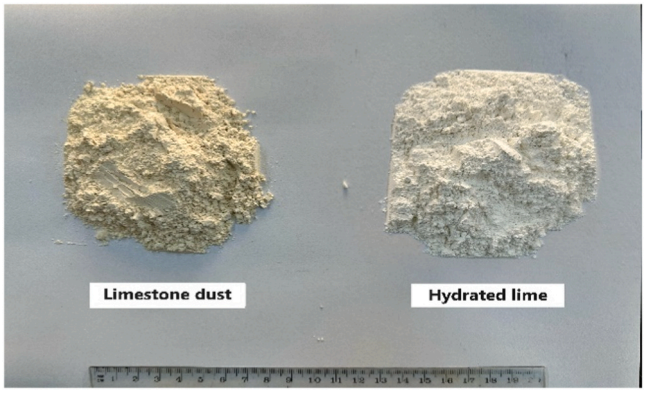

Fig. A1. The filler materials.

.

Fig. A1. Shows the appearance and the used states of the two filler materials. Fig. A2 gives out the SEM images at magnification level of 2 K. The SEM examination unveils the distinctive difference between the particles of the two fillers. The limestone dust particles demonstrate an angular crystalline structure with a rough surface, a typical character of the calcite, which helps enhance mechanical interlocking when used as a filler. On contrast, the hydrated lime particles display a more amorphous and irregular arrangement with a smoothly flocculated texture, a character of a substantial specific surface area, which plays the main role improving the performance of concrete mixes using the filler. The smoother surface texture of hydrated lime particles, due to the chemical hydration process, benefits better adhesion and reactivity when mixed with asphalt cement to enhance the performance of the binder.

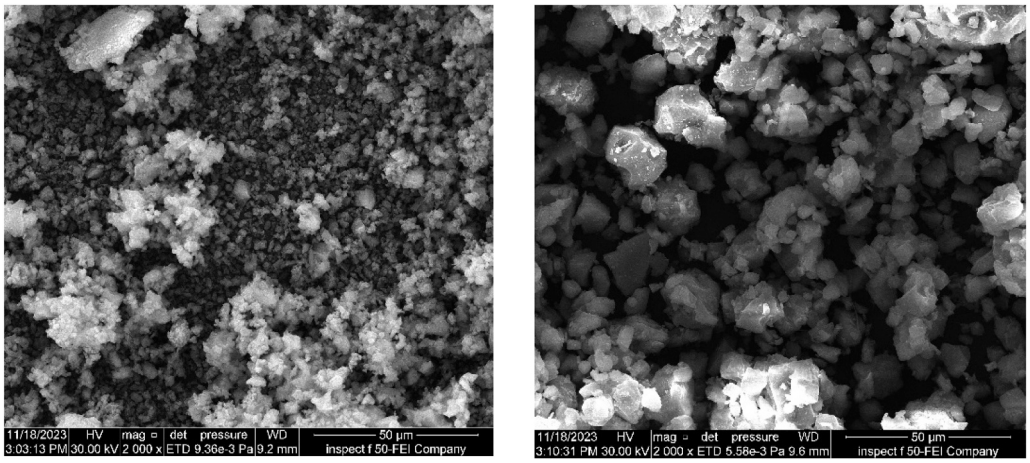

Fig. A2. SEM for the two types of fillers.

.

References

[1] K. Zhang, W. Xie, Y.-L. Zhao, Permanent deformation characteristic of asphalt mixture under coupling effect of moisture, overload and loading frequency, Constr. Build. Mater. 272 (22) (2021) 121985.

[2] Y.-F. Du, J.-Q. Chen, Z. Han, W.-Z. Liu, A review on solutions for improving rutting resistance of asphalt pavement and test methods, Constr. Build. Mater. 168 (2018) 893–905.

[3] J.-T. Fan, Y.-J. Jiang, Y. Yi, T. Tian, K.-J. Yuan, C.-Q. Deng, Investigation on triaxial numerical test method and dilatancy behavior of asphalt mixture, Constr. Build. Mater. 316 (2022) 125815.

[4] R. Guo, T.-F. Nian, F. Zhou, Analysis of factors that influence anti-rutting performance of asphalt pavement, Constr. Build. Mater. 254 (2020) 119237.

[5] Y.-J. Jiang, Y. Yi, J.-T. Fan, T. Tian, C.Q. Deng, Laboratory investigation on the heat dissipation regularity and road performance of different pavement structure combinations by double-layer paving, Constr. Build. Mater. 284 (2021) 122785.

[6] F. Wang, Y. Xiao, Z.-W. Chen, P.-D. Cui, J. Liu, N. Wang, Morphological characteristics of mineral filler and their influence on active adhesion between aggregates and bitumen, Constr. Build. Mater. 323 (14) (2022) 126520.

[7] A.F. Al-Tameemi, Y. Wang, A. Albayati, Experimental study of the performance related properties of the asphalt concrete modified with hydrated lime, J. Mater. Civ. Eng. 28 (5) (2016) 04015185.

[8] A.F. Al-Tameemi, Y. Wang, A. Albayati, J. Haynes, Moisture susceptibility and fatigue performance of hydrated lime–modified asphalt concrete: experiment and design application case study, J. Mater. Civ. Eng. 31 (4) (2019) 04019019.

[9] Q.-H. Wei, Al Ashaibi, A. Wang, Y. Albayati, A. Haynes J, Experimental study of temperature effect on the mechanical tensile fatigue of hydrated lime modified asphalt concrete and case application for the analysis of climatic effect on constructed pavement, Case Stud. Constr. Mater. 17 (2022) e01622.

[10] O.V. Laukkanen, H. Soenen, T. Pellinen, S. Heyrman, G. Lemoine, Creep-recovery behavior of bituminous binders and its relation to asphalt mixture rutting, Mater. Struct. 48 (2015) 4039–4053.

[11] D. Singh, A.V. Kataware, Comparison of different rheological parameters for rutting susceptibility of SBS+WMA modified binders, Innov. Infrastruct. Solut. 1 (2016) 28.

[12] D.B. McLean, C.L. Monismith, Estimation of Permanent Deformation in Asphalt Concrete Layers Due to Repeated Traffic Loading, Transp. Res. Rec. 510, Transp. Res. Board (1974) (Washington, D.C).

[13] M.R. Islam, S.A. Kalevela, S.K. Nesselhauf, Sensitivity of the Flow Number to Mix Factors of Hot-Mix Asphalt, Infrastructures 4 (2) (2019) 34.

[14] Bonaquist R. Evaluation of Flow Number (Fn) as a Discriminating HMA Mixture Property, Advanced Asphalt Technologies, LLC, WHRP 12–01, 2012, Wisconsin Highway Research Program University of Wisconsin-Madison.

[15] J.-T. Zhang, J. Yang, J. Han, W.G. Zhang, Evaluation of Dilatancy Behavior of Asphalt Mixtures Using Partial Triaxial Compression Tests, J. Mater. Civ. Eng. 28 (1) (2016).

[16] T.-Y. Zhu, T. Ma, X.-M. Huang, S.-Q. Wang, Evaluating the rutting resistance of asphalt mixtures using a simplified triaxial repeated load test, Constr. Build. Mater. 116 (2016) 72–78.

[17] B. Huang, Y.-T. Zhang, T. Qi, H.-X. Han, Static and Dynamic Properties and Temperature Sensitivity of Emulsified Asphalt Concrete, Adv. Mater. Sci. Eng. (2018) 7067608.

[18] W. Fedrigo, W.P. Núñez, M.A.C. López, T.R. Kleinert, J.A.P. Ceratti, A study on the resilient modulus of cement-treated mixtures of RAP and aggregates using indirect tensile, triaxial and flexural tests, Constr. Build. Mater. 171 (2018) 161–169.

[19] T. Huang, S. Qi, H. Liu, H. Yu, S. Li, Shear Properties of Asphalt Mixtures under Triaxial Compression, Appl. Sci. 9 (2019) 1489.

[20] P.E. Sebaaly, E. Hitti, D. Weitzel, Effectiveness of Lime in Hot-Mix Asphalt Pavements, Transp. Res. Rec.: J. Transp. Res. Board 1832 (1) (2003).

[21] S. Bourona, F. Hammouma, H. Ruatb, P. Métaisc, D. Lesueurc, Case study - improving the durability of asphalt mixtures with hydrated lime: field results from highway A84, Case Stud. Constr. Mater. 14 (2021) e00551.

[22] H. Taherkhani, M. Tajdini, Comparing the effects of nano-silica and hydrated lime on the properties of asphalt concrete, Constr. Build. Mater. 218 (2019) 308–315.

[23] M. Lagos-Varas, et al., Viscoelasticity modelling of asphalt mastics under permanent deformation through the use of fractional calculus, Constr. Build. Mater. 329 (25) (2022) 127102.

[24] ASTM. Standard practice for preparation of bituminous specimens using Marshall apparatus. ASTM D6926–10, (2010). West Conshohocken, PA.

[25] W.H. Goetz, J.H. SCHAUB, Triaxial Testing of Bituminous Mixtures, Technical Report, Purdue University,, 1959.

[26] P. Orosa, I. Perez, A.R. Pasandín, Evaluation of the shear and permanent deformation properties of cold in-place recycled mixtures with bitumen emulsion using triaxial tests, Constr. Build. Mater. 328 (2022) 127054.

[27] Xua Y., Suna L.-J. Study on permanent deformation of asphalt mixtures by single penetration repeated shear test, 13th COTA International Conference of Transportation Professionals (CICTP 2013), Procedia - Social and Behavioral Sciences 2013, 96: 886 – 893.

[28] H.S. Yu, J. Wang, Three-dimensional shakedown solutions for cohesive frictional materials under moving surface loads, Int. J. Solids Struct. 49 (2012) 3797–3807.

[29] S. Liu, J. Wang, H.S. Yu, D. Wanatowski, N. Thom, J. Grenfell, Shakedown of asphalt pavements considering temperature effect, Int. J. Pavement Eng. 23 (5) (2022) 1572–1583.

[30] Jacob Uzan, Resilient characterization of pavement materials, Intern. Jo~ J. Rnalfo R. Numer. Anal. Methods Geomech. Vol. 16 (1992) 453–459.

[31] F. Zeng, L. Shao, Unloading elastic behavior of sand in cyclic triaxial tests, Geotech. Test. J. (2016), https://doi.org/10.1520/GTJ20150171.

[32] A. Sağlik, A.G. Gungor, Resilient modulus of unbound and bituminous bound road materials. 5th Eurasphalt & Eurobitume Congress, Istanbul,, 2012.

[33] B. Shackel, The Derivation of Complex Stress-Strain Relations, in: *Proc. 8th Int. Conf. Soil Mech. Found.* Eng, Vol. 1, Moscow,, 1973, pp. 353–359.

[34] A.A. Ashaibi, Y. Wang, A. Albayati, J. Byzyka, M. Scholz, L. Weekes, Thermal properties of hydrated lime-modified asphalt concrete and modelling evaluation for their effect on the constructed pavements in service, Sustainability 14 (2022) 7827.

[35] J. Busby, UK shallow ground temperatures for ground coupled heat exchangers, Q. J. Eng. Geol. Hydrogeol. 48 (2015) 248–260.